Theoretical and Numerical Studies of Wire Mesh Structures

D.A. Hill and J.R. Wait

Institute for Telecommunication Sciences
Office of Telecommunications
U.S. Department of Commerce
Boulder, Colorado 80302

ABSTRACT

The electromagnetic scattering of a plane wave by a rectangular wire mesh is analyzed in both a free space and a half-space environment. Plane wave reflection and transmission coefficients are computed to illustrate the dependence of wire mesh performance on the numerous important parameters. The case of plane wave excitation is also extended to surface wave propagation and dipole radiation patterns.

TABLE OF CONTENTS

ILLUSTRATIONS

4

SECTION I

INTRODUCTION

This report consists of four sections (II-V) which deal with electro-
magnetic scattering by wire mesh structures. Here we summarize what has
been done, how the various sections are related, and what problems remain
to be solved.

Section II considers the plane wave scattering by a square wire mesh
with bonded junctions. Such square, bonded meshes are frequently used for
ground screens and in other shielding applications. A special junction
treatment was found necessary to efficiently analyze a bonded mesh, and
numerical results for plane wave reflection and transmission coefficients
are presented to illustrate the effect of various parameters on mesh per-
formance.

Section III utilizes the formulation developed in Section II in order
to treat surface wave propagation over a square, bonded mesh. This is an
important problem since surface waves can be excited by realistic sources,
such as a vertical dipole antenna. Numerical results are presented for the
propagation constant as a function of various parameters. The similarity of
this propagation constant to that of a plane wave in free space is a measure
of the shielding effectiveness of the mesh.

In order to examine a more realistic model for antenna ground screens,
Section IV considers a wire mesh over a lossy half-space. The treatment is
only rigorously valid for unbonded meshes, but for square meshes the results
for incidence along the mesh diagonal ($\phi = 45^\circ$) are also representative of

a bonded mesh. Numerical results for the plane wave reflection coefficients are presented in order to illustrate the effect of various parameters.

Section V is primarily an extension of Section IV with numerous additional numerical results presented. The results for a mesh very close to the ground should also be valid for the practical case of a mesh lying on the ground or even slightly buried. Numerical results for rectangular meshes are presented, and they are found to agree with the method of averaged boundary conditions developed by the Soviets for small mesh sizes. Also considered in Section V are the radiation patterns of short electric dipoles of arbitrary orientation, located above a mesh. The numerical results are applicable to scattering by a test object (by giving an indication of how the image fields are modified) as well as source radiation for frequencies high enough to satisfy far field criteria.

The main geometry which remains to be analyzed is the bonded, rectangular mesh either in free space or above a half space. This type of mesh has been used, and there are some questions regarding the appropriate cross-wire spacing. As well as plane wave reflection, surface wave propagation along this type of structure is also of interest. The propagation constant in the half space geometry would be complex since the lossy earth would introduce attenuation. Some numerical results would be useful in quantifying the importance of attenuation of the high frequency components Electromagnetic Pulse (EMP) simulators.

SECTION II

ELECTROMAGNETIC SCATTERING OF AN ARBITRARY PLANE
.WAVE BY A WIRE MESH WITH BONDED JUNCTIONS

INTRODUCTION

The electromagnetic properties of a single planar array of parallel
wires have been investigated extensively in both a free space environment
(refs. 1-5) and for various half-space environments (refs. 6-10). The wire
mesh screen has received less attention, and some disagreements on the
properties of such screens still exist.

The reflecting and transmitting properties of both square meshes
(ref. 11) and rectangular meshes (ref. 12) have been calculated by using
the method of averaged boundary conditions (ref. 13). The method appears
to give good results for both bonded and unbonded junctions, but is only
valid for mesh dimensions which are small compared with a wavelength.
Otteni (ref. 14) has presented a general solution to the problem which re-
quires matrix inversion to determine the mesh currents and resultant re-
flection coefficients. However, his results are in disagreement with those
of Kontorovich et al. (ref. 11) and Astrahan (ref. 12) who predict no azi-
muthal dependence for the properties of bonded meshes.

A general solution has also been given for plane wave scattering from
separated wire grids (ref. 15). The planar grid separation was allowed to
become small as in an unbonded mesh, but the bonded mesh limit was not con-
sidered. Here we extend the previous solution to the bonded mesh case by
setting the separation equal to zero and making slightly different approxi-
mations. No special junction conditions on the current or charge at the
junction are found necessary, but convergence of the solution is found to
be extremely slow resulting in the need for inversion of very large matrices.
Our convergence calculations indicate that some of the results of Otteni

8

(ref. 14) are incorrect because he has not taken enough terms in his current expansion to obtain convergence.

The primary reason for slow convergence in the bonded mesh problem is that the Fourier series expansion for the current is inefficient in synthesizing the current jump which occurs at the wire junction. We find that by adding the proper jump function to the Fourier series representation, the required number of current expansion coefficients is reduced by a factor of about ten, and the required computer time is reduced by more than a factor of one hundred. Using this improved solution, numerical results for current distributions and reflection and transmission coefficients are obtained. For simplicity, we consider a square mesh with perfectly conducting wires, but the technique is also applicable to rectangular meshes with imperfectly conducting wires.

FORMULATION

The geometry is illustrated in Fig. 1. Arrays of wires parallel to the x and y axes with spacing a are located in the plane $z = 0$, and perfect contacts are made at the junctions. The wire radius c is small compared to both the spacing a and the free space wavelength λ. Consequently, the wires carry only axial currents, and the usual thin-wire approximations are valid.

The incident electric field $\bar{E}_{inc}$ is an arbitrarily polarized plane wave:
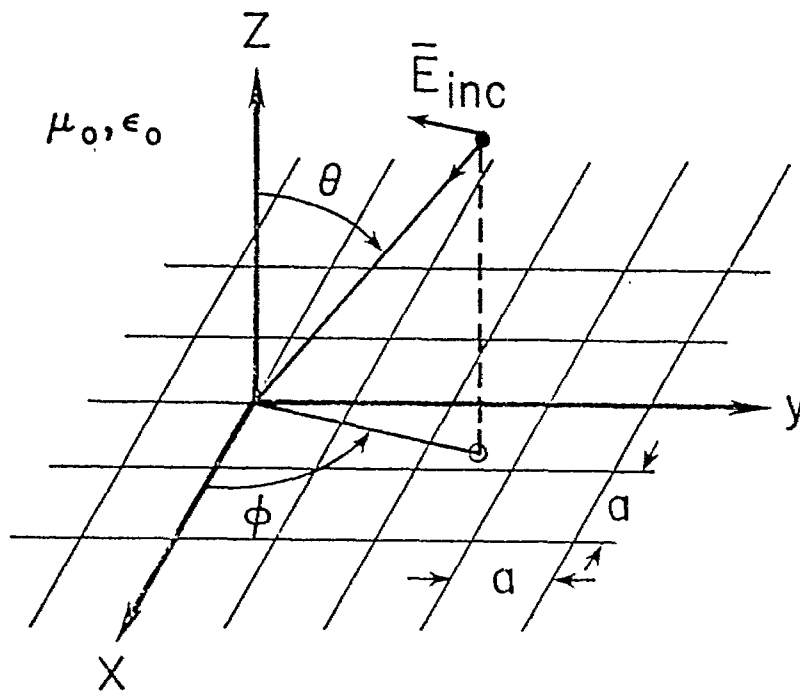
Figure 1.   Geometry for a plane wave of arbitrary polarization incident on a
wire mesh with bonded junctions. Wire radius equals c.

10

$$\bar{E}_{inc} = \bar{E}_o \exp\{ik[z \cos\theta + \sin\theta \ (x \cos\phi + y \sin\phi)]\} \qquad (1)$$

where $\bar{E}_o$ is the incident field at the origin, $k(= 2\pi/\lambda)$ is the free space wavenumber, and ϕ and θ are the azimuthal and elevation incidence angles. The time dependence is $\exp(i\omega t)$.

From Floquet's theorem *(ref. 16)*, the wire currents for the qth x-directed wire I_{xq} and the mth y-directed wire I_{ym} can be written as periodic functions multiplied by the phase dependence of the incident field in (1):

$$I_{xq} = \sum_{m=-\infty}^{\infty} A_m \exp\{i[2\pi mx/a + k \sin\theta (x \cos\phi + qa \sin\phi)]\}$$

$$\qquad (2)$$

$$I_{ym} = \sum_{q=-\infty}^{\infty} B_q \exp\{i[2\pi qy/a + k \sin\theta (y \sin\phi + ma \cos\phi)]\}$$

The fields scattered by the wires can be derived from a magnetic vector potential which has only x and y components. In order to solve for the unknown coefficients A_m and B_q, we set the total tangential electric field equal to zero at the tops of the wires: $E_{x,\ total} = 0$ at $y = 0$ and $z = c$ and $E_{y,\ total} = 0$ at $x = 0$ and $z = c$. From these conditions, a doubly infinite set of linear equations can be obtained for A_m and B_q *(ref. 15)*. The procedure is equivalent to a method of moments solution of Pocklington's equation for thin wires *(ref. 17)* using entire domain sinusoidal expansion and testing functions. Specializing the solution of Hill and Wait *(ref. 15)* to the bonded square mesh with perfectly conducting wires, we obtain the following doubly infinite set of linear equations:

$$\delta_{mo}E_{ox}\exp(ikc\cos\theta) - A_m\left\{\frac{i\omega\mu_o}{2k^2a}\left[k^2 - \left(\frac{2\pi m}{a} + k\sin\theta\cos\phi\right)^2\right]S_m\right\}$$

$$+ \frac{i\omega\mu_o}{2k^2a}\left(\frac{2\pi m}{a} + k\sin\theta\cos\phi\right)\sum_q B_q\left(\frac{2\pi q}{a} + k\sin\theta\sin\phi\right)\frac{\exp(-\Gamma_{mq}c)}{\Gamma_{mq}} = 0$$

$$\delta_{qo}E_{oy}\exp(ikc\cos\theta) - B_q\left\{\frac{i\omega\mu_o}{2k^2a}\left[k^2 - \left(\frac{2\pi q}{a} + k\sin\theta\sin\phi\right)^2\right]S'_q\right\}$$

$$\text{(3)}$$

$$+ \frac{i\omega\mu_o}{2k^2a}\left(\frac{2\pi q}{a} + k\sin\theta\sin\phi\right)\sum_m A_m\left(\frac{2\pi m}{a} + k\sin\theta\cos\phi\right)\frac{\exp(-\Gamma_{mq}c)}{\Gamma_{mq}} = 0$$

where $\Gamma_{mq} = [(2\pi m/a + k\sin\theta\cos\phi)^2 + (2\pi q/a + k\sin\theta\sin\phi)^2 - k^2]^{\frac{1}{2}}$

$$S_m = \sum_q \frac{\exp(-\Gamma_{mq}c)}{\Gamma_{mq}}, \qquad S'_q = \sum_m \frac{\exp(-\Gamma_{mq}c)}{\Gamma_{mq}}$$

$$\delta_{mn} = \begin{cases} 1, & m = n \\ 0, & m \neq n \end{cases}$$

and E_{ox} and E_{oy} are the x and y components of the incident electric field at the origin. All summations are taken to run from $-\infty$ to ∞ unless otherwise stated. The factor $\exp(ikc\cos\theta)$ which multiplies the incident fields in (3) was dropped in the previous treatment because it is near unity. The convergence of the summations S_m and S'_q can be improved as was done previously (ref. 15), but some of the previous approximations cannot be made here because large values of m and q are required for convergence of (3). For S_m, we have:

12

$$S_m = {\sum_q}' \left[\frac{\exp(-\Gamma_{mq}c)}{\Gamma_{mq}} - \frac{\exp(-2\pi|q|c/a)}{|2\pi q/a|} \right]$$

$$+ \frac{a}{2\pi} {\sum_q}' \frac{\exp(-2\pi|q|c/a)}{|q|} + \frac{\exp(-\Gamma_{mo}c)}{\Gamma_{mo}}$$

(4)

$$= \frac{a}{\pi} \left\{ - \ln\left[1 - \exp\left(\frac{-2\pi c}{a} \right) \right] + \Delta_m \right\} + \frac{\exp(-\Gamma_{mo}c)}{\Gamma_{mo}}$$

where
$$\Delta_m = \frac{1}{2} {\sum_q}' \left[\frac{2\pi}{a} \frac{\exp(-\Gamma_{mq}c)}{\Gamma_{mq}} - \frac{\exp(-2\pi|q|c/a)}{|q|} \right]$$

and ' on $\sum$ indicates omission of the $q = 0$ term. The term Δ_m converges rapidly and is easily summed on a computer. In a similar manner for S_q', we have:

$$S_q' = \frac{a}{\pi} \left\{ - \ln\left[1 - \exp\left(\frac{-2\pi c}{a} \right) \right] + \delta_q \right\} + \frac{\exp(-\Gamma_{oq}c)}{\Gamma_{oq}}$$

(5)

where
$$\delta_q = \frac{1}{2} {\sum_m}' \left[\frac{2\pi}{a} \frac{\exp(-\Gamma_{mq}c)}{\Gamma_{mq}} - \frac{\exp(-2\pi|m|c/a)}{|m|} \right]$$

The solution of (3) is discussed in the following section.

The transmission and reflection coefficients are the quantities of most interest in characterizing the mesh. In order to define these coefficients, it is first necessary to specify the incident electric field. For θ (vertical or TM) polarization, the incident electric field has a θ component E_θ^{inc} given by

$$E_\theta^{inc} = E_{o\theta} \exp\{ik[z\cos\theta + \sin\theta(x\cos\phi + y\sin\phi)]\}$$

(6)

Consequently, the x and y components at the origin which are required in (3) to solve for the current coefficients are given by:

13

$$E_{ox} = E_{o\theta} \cos\theta\cos\phi, \quad E_{oy} = E_{o\theta} \cos\theta\sin\phi \tag{7}$$

For ϕ (horizontal or TE) polarization, the incident electric field has a ϕ component E_ϕ^{inc} given by

$$E_\phi^{inc} = E_{o\phi} \exp\{ik[z\cos\theta + \sin\theta(x\cos\phi + y\sin\phi)]\} \tag{8}$$

Consequently, E_{ox} and E_{oy} for ϕ polarization are:

$$E_{ox} = -E_{o\phi} \sin\phi, \quad E_{oy} = E_{o\phi} \cos\phi \tag{9}$$

For a less than $\lambda/2$, there are no grating lobes, and only the constant current components, A_o and B_o, contribute to the scattered far field. The rectangular components of the scattered field for large negative z are given by (ref. 15):

$$E_x^{s-} = \frac{-\eta_o}{2a\cos\theta} [A_o(1 - \sin^2\theta\cos^2\phi) - B_o\sin^2\theta\sin\phi\cos\phi]$$

$$\cdot \exp\{ik[z\cos\theta + \sin\theta(x\cos\phi + y\sin\phi)]\}$$

$$E_y^{s-} = \frac{\eta_o}{2a\cos\theta} [A_o\sin^2\theta\sin\phi\cos\phi - B_o(1 - \sin^2\theta\sin^2\phi)]$$

$$\tag{10}$$

$$\cdot \exp\{ik[z\cos\theta + \sin\theta(x\cos\phi + y\sin\phi)]\}$$

$$E_z^{s-} = \frac{\eta_o\sin\theta}{2a} [A_o\cos\phi + B_o\sin\phi] \exp\{ik[z\cos\theta$$

$$+ \sin\theta(x\cos\phi + y\sin\phi)]\}$$

14

where $\eta_o = (\mu_o/\varepsilon_o)^{\frac{1}{2}}$.

The θ and ϕ components of the scattered field are:

$$E_\theta^{s-} = -E_z^{s-} \sin\theta + E_x^{s-} \cos\theta\cos\phi + E_y^{s-} \cos\theta\sin\phi \qquad (11)$$

and

$$E_\phi^s = -E_x^{s-}\sin\phi + E_y^{s-}\cos\phi$$

For θ polarization, the parallel and cross-polarized transmission coefficients ($T_{\theta\theta}$ and $T_{\theta\phi}$) are defined as

$$T_{\theta\theta} = 1 + E_\theta^{s-}/E_\theta^{inc} \quad \text{and} \quad T_{\theta\phi} = E_\phi^{s-}/E_\theta^{inc} \qquad (12)$$

For ϕ polarization, the parallel and cross-polarized transmission coefficients ($T_{\phi\phi}$ and $T_{\phi\theta}$) are defined as

$$T_{\phi\phi} = 1 + E_\phi^{s-}/E_\phi^{inc} \quad \text{and} \quad T_{\phi\theta} = E_\theta^{s-}/E_\phi^{inc} \qquad (13)$$

The reflection coefficients are determined from the scattered field evaluated at large positive values of z. In this case, the scattered rectangular components are the same as those in (10) except for a sign change in z in the exponents and a sign change in the z component

$$E_x^{s+} = E_x^{s-}\bigg|_{z=-z} \quad , \quad E_y^{s+} = E_y^{s-}\bigg|_{z=-z}$$

$$(14)$$

and

$$E_z^{s+} = -E_z^{s-}\bigg|_{z=-z}$$

15

The θ and ϕ components of the scattered field for large positive z are:

$$E_\theta^{s+} = -E_z^{s+} \sin\theta - E_x^{s+} \cos\theta\cos\phi - E_y^{s+} \cos\theta\sin\phi$$

(15)

and
$$E_\phi^{s+} = -E_x^{s+} \sin\phi + E_y^{s+}\cos\phi$$

For θ polarization, the parallel and cross-polarized reflection coefficients ($R_{\theta\theta}$ and $R_{\theta\phi}$) are defined as:

$$R_{\theta\theta} = E_\theta^{s+} \exp\{-ik[-z\cos\theta + \sin\theta(x\cos\phi + y\sin\phi)]\}/E_{o\theta}$$

(16)

$$R_{\theta\phi} = E_\phi^{s+} \exp\{-ik[-z\cos\theta + \sin\theta(x\cos\phi + y\sin\phi)]\}/E_{o\theta}$$

For ϕ polarization, the parallel and cross-polarized reflection coefficients ($R_{\phi\phi}$ and $R_{\phi\theta}$) are defined as:

$$R_{\phi\phi} = E_\phi^{s+} \exp\{-ik[-z\cos\theta + \sin\theta(x\cos\phi + y\sin\phi)]\}/E_{o\phi}$$

(17)

$$R_{\phi\theta} = E_\theta^{s+} \exp\{-ik[-z\cos\theta + \sin\theta(x\cos\phi + y\sin\phi)]\}/E_{o\phi}$$

The exponential factors in (16) and (17) simply refer the phase to the origin.

Since we are considering the case of lossless wires and mesh spacings less than a half wavelength, all incident energy is either transmitted or reflected, and energy conservation can be used to provide a consistency check for the calculations. For θ polarization, the necessary condition is:

$$|T_{\theta\theta}|^2 + |T_{\theta\phi}|^2 + |R_{\theta\theta}|^2 + |R_{\theta\phi}|^2 = 1$$

(18)

16

For ϕ polarization, the necessary condition is

$$\left|T_{\phi\phi}\right|^2 + \left|T_{\phi\theta}\right|^2 + \left|R_{\phi\phi}\right|^2 + \left|R_{\phi\theta}\right|^2 = 1 \tag{19}$$

NUMERICAL SOLUTION

In order to solve the doubly infinite set of equations in (3) for the current coefficients A_m and B_q, the equations were truncated and solved by matrix inversion. A computer program was written which was capable of inverting a matrix of order 126×126 ($m,q = -31,\ldots,0,\ldots 31$). The accuracy of the matrix inversion was verified by obtaining good agreement between single and double precision inversion. Convergence was examined by increasing the matrix order in steps and observing the change in the dominant current coefficients A_o and B_o. This is roughly equivalent to observing the change in the reflection and transmission coefficients. We define convergence as having been obtained when a further increase in the matrix order $(N \times N)$ produces a negligible change in A_o and B_o (or in the reflection and transmission coefficients). A number of cases were studied numerically, and for θ polarization, convergence was found to be extremely slow for incidence along a wire axis ($\phi = 0°$) and near grazing (θ near $90°$). Conversely, convergence is found to be very rapid for ϕ near $45°$ (all θ) or for θ near $0°$ (all ϕ). This qualitative behavior is in agreement with Otteni *(ref. 14)* whose program was written for θ polarization for a matrix order up to 70×70. However, we find that, for cases where convergence is slow, a much larger matrix order is required than that predicted by Otteni. Convergence is quite fast for ϕ polarization for all incidence angles.

In order to illustrate the convergence difficulties, we consider the following case for θ polarization: $a/\lambda = 0.25$, $c/a = 0.02$, $\theta = 70°$, and $\phi = 0°$. This case is chosen because a measured value of the transmission

17

coefficient is available (ref. 11). The convergence of $|T_{\theta\theta}|$ as a function of N is shown in Fig. 2, and the final value is seen to agree closely with the measured value of Kontorovich, et al. (ref. 11). The cross-polarized transmission coefficient $T_{\theta\phi}$ is zero by symmetry in this case since $\phi = 0°$. For comparison, the rapid convergence for a planar separation h of 3 wire radii for the x and y directed arrays as computed by the previous formulation for unbonded wires (ref. 15) is also shown in Fig. 2 along with the experimental value of Kontorovich et al. (ref. 11). Although the agreement is fairly good, an exact comparison is not expected because the unbonded wires in the experiment were touching and some finite junction impedance probably existed.

In order to understand why the convergence is so slow for the bonded case in Fig. 2, it is useful to examine the current distribution on the wires for the same case as given by Fig. 2. For a given value of N, the summations on m and q run from $-(N-2)/4$ to $(N-2)/4$. Consequently, the summations run from -30 to 30 for $N = 122$. The resultant real and imaginary parts of I_{xo} and I_{yo} are shown for one Floquet cell $(-a/2 < x < a/2, -a/2 < y < a/2)$ in Fig. 3. It is seen that the current waveforms suffer from Gibbs' phenomenon (ref. 18) near the junction $(x=y=0)$ where a step discontinuity is expected in both I_{xo} and I_{yo}. This difficulty does not occur for the unbonded mesh where the current is continuous, and the resultant convergence is much more rapid as seen in Fig. 2.

If the jump discontinuities in I_{xo} and I_{yo} are estimated from the waveforms in Fig. 3, it is found that the jumps are the negatives of each other. Consequently, Kirchhoff's current law has been satisfied:

18
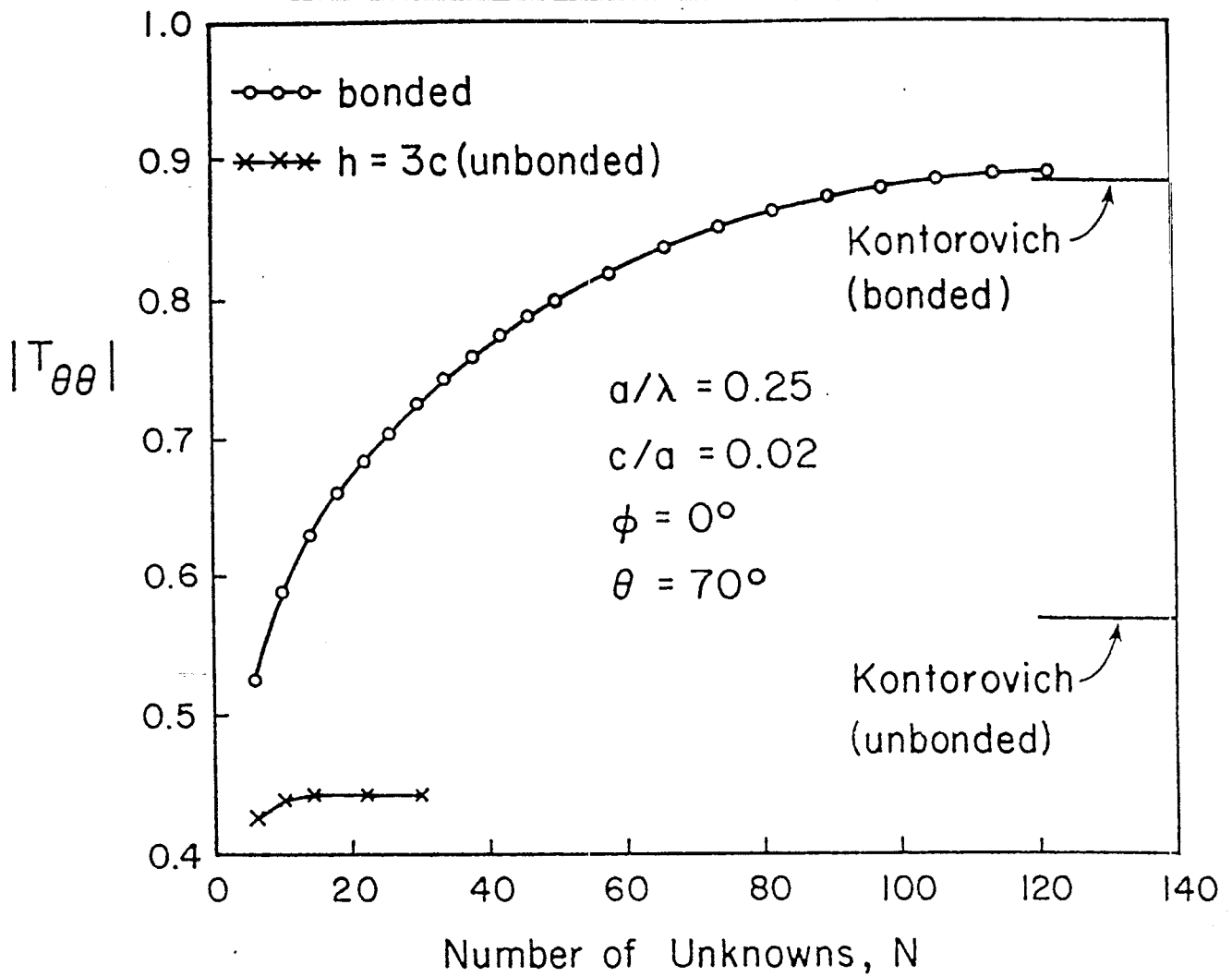
Figure 2. Convergence for bonded and unbonded meshes. The experimental values of Kontorovich et al. (ref. 11) are shown for comparison.
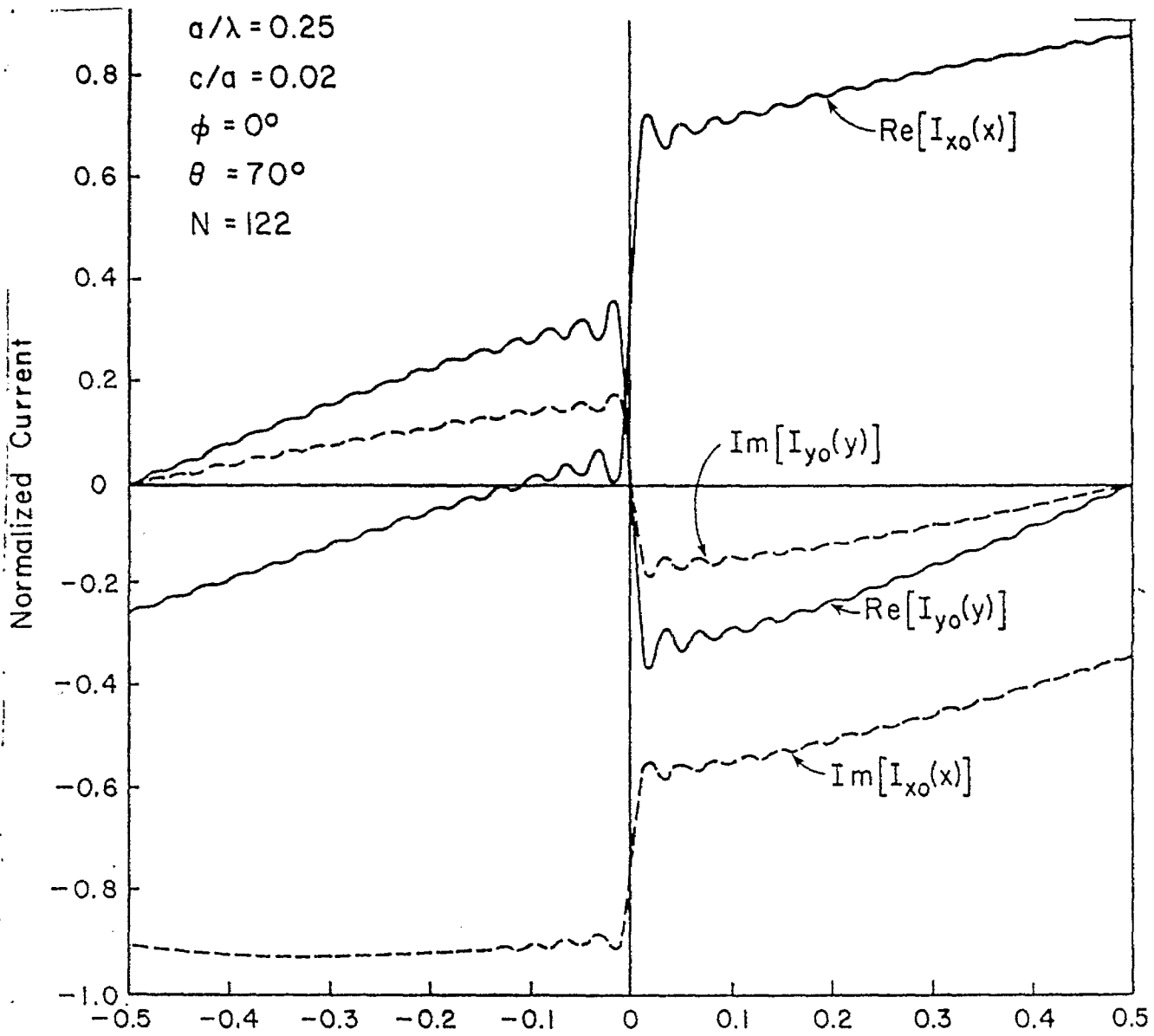
Figure 3. Normalized current waveforms for one Floquet cell. (The normalization factor is $E_o\theta a/\eta_o$.

20

$$I_{xo}(0^+) - I_{xo}(0^-) + I_{yo}(0^+) - I_{yo}(0^-) = 0 \qquad (20)$$

This is a partial check on the accuracy of the solution. In a finite difference treatment of Pocklington's equation for a pair of crossed wires, Mittra and Ko (ref. 19) have recently shown, that Kirchoff's current law is, in fact, satisfied if the proper sampling interval is used. Thus, in principle, it appears that junction conditions do not necessarily have to be enforced in crossed wire problems. Furthermore, from charge continuity, King and Wu (ref. 20) have derived the following additional conditions for crossed wires of equal radii:

$$\frac{\partial I_{xo}}{\partial x}\bigg|_{x=0^-} = \frac{\partial I_{xo}}{\partial x}\bigg|_{x=0^+} = \frac{\partial I_{yo}}{\partial y}\bigg|_{y=0^-} = \frac{\partial I_{yo}}{\partial y}\bigg|_{y=0^+} \qquad (21)$$

The Gibbs' phenomenon oscillations in Fig. 3 make the current slopes difficult to estimate, but it appears that (21) is roughly satisfied if average slopes are used. Actually, good agreement for current waveforms has been obtained by a number of investigators (refs. 19 and 21-23) even when (21) is not well satisfied.

Numerical results for other cases show that as in Fig. 2 large matrices are required for convergence, but that Kirchhoff's current law is satisfied. Thus a direct solution of (3), without enforcement of junction conditions, is a valid procedure but excessive computer time is required.

IMPROVED SOLUTION

The primary reason for the slow convergence of the truncated system of equations (3) is that the continuous functions in the current expansions in (2) are inefficient in synthesizing the discontinuous current which

occurs for the bonded mesh. This problem could be eliminated by using discontinuous expansion functions for the current (such as pulses), but then the resultant equations would be much more complicated than those in (3). A more efficient scheme is suggested by the fact that the higher order coefficients for I_{xo} and I_{yo} are observed to fall off linearly with an amplitude determined only by the jump at the junction. Thus, we define the following jump function $f_\Delta(x)$:

$$f_\Delta(x) = \frac{\Delta}{2\pi i} \sum_n{}' \frac{\exp(i2\pi nx/a)}{n}$$

(22)

$$= \Delta\left[U(x) - \frac{x}{a} - \frac{1}{2}\right] , \quad -\frac{a}{2} < x < \frac{a}{2}$$

where
$$U(x) = \begin{cases} 1, & x > 0 \\ 0, & x < 0 \end{cases}$$

Note that f_Δ is a sawtooth function with a jump of Δ at the origin and that I_{yo} in Fig. 2 has a similar shape.

Using (22), it is possible to write the currents in the following form which is still equivalent to (2):

$$I_{xq}(x) = \exp[ik\sin\theta(x\cos\phi + qa\sin\phi)]$$

$$\cdot \left[f_\Delta(x) + \sum_m A'_m \exp\left(\frac{i2\pi mx}{a}\right)\right]$$

(23)

$$I_{ym}(y) = \exp[ik\sin\theta(y\sin\phi + ma\cos\phi)]$$

$$\cdot \left[-f_\Delta(y) + \sum_m B'_q \exp\left(\frac{i2\pi qy}{a}\right)\right]$$

22

where
$$A'_m = A_m - \frac{\Delta(1 - \delta_{mo})}{2\pi im}$$

and
$$B'_q = B_q + \frac{\Delta(1 - \delta_{qo})}{2\pi iq}$$

Note that equal and opposite jumps are now built into the x and y directected currents and Kirchhoff's law is automatically satisfied. Note that (23) is actually obtained by replacing A_m and B_q by

$$A_m = A'_m + \frac{\Delta(1 - \delta_{mo})}{2\pi im}$$

$$\text{(24)}$$

and
$$B_q = B'_q - \frac{\Delta(1 - \delta_{qo})}{2\pi iq}$$

In order to derive the new set of equations equivalent to (3), we substitute (24) into (3) and obtain the following:

$$\delta_{mo}E_{ox}\exp(ikc\cos\theta) - A'_m \left\{ \frac{i\omega\mu_o}{2k^2a} \left[k^2 - \left(\frac{2\pi m}{a} + k\sin\theta\cos\phi \right)^2 \right] S_m \right\}$$

$$+ \frac{i\omega\mu_o}{2k^2a} \left(\frac{2\pi m}{a} + k\sin\theta\cos\phi \right) \sum_q B'_q \left(\frac{2\pi q}{a} + k\sin\theta\sin\phi \right) \frac{\exp(-\Gamma_{mq}c)}{\Gamma_{mq}}$$

$$\text{(25)}$$

$$+ \Delta \left\{ \frac{(\delta_{mo} - 1)}{2\pi mi} \frac{i\omega\mu_o}{2k^2a} \left[k^2 - \left(\frac{2\pi m}{a} + k\sin\theta\cos\phi \right)^2 \right] S_m \right.$$

$$\left. - \frac{i\omega\mu_o}{2k^2a} \left(\frac{2\pi m}{a} + k\sin\theta\cos\phi \right) \left[\frac{S_m}{ia} + \frac{k\sin\theta\sin\phi}{2\pi i} S_{1m} \right] \right\} = 0$$

$$\delta_{qo}E_{oy}\exp(ikc\cos\theta) - B'_q \left\{ \frac{i\omega\mu_o}{2k^2a} \left[k^2 - \left(\frac{2\pi q}{a} + k\sin\theta\sin\phi \right)^2 \right] S'_q \right\}$$

$$+ \frac{i\omega\mu_o}{2k^2a} \left(\frac{2\pi q}{a} + k\sin\theta\sin\phi \right) \sum_m A'_m \left(\frac{2\pi m}{a} + k\sin\theta\cos\phi \right) \frac{\exp(-\Gamma_{mq}c)}{\Gamma_{mq}}$$

22-A

$$+ \Delta \left\{ \frac{(1 - \delta_{qo})}{2\pi q i} \frac{i\omega\mu_o}{2k^2 a} \left[k^2 - \left(\frac{2\pi q}{a} + k\sin\theta\sin\phi \right)^2 \right] S_q' \right.$$

$$\left. + \frac{i\omega\mu_o}{2k^2 a} \left(\frac{2\pi q}{a} + k\sin\theta\sin\phi \right) \left[\frac{S_q'}{ia} + \frac{k\sin\theta\cos\phi}{2\pi i} S_{1q}' \right] \right\} = 0$$

$$S_{1m} = \sum_q {}' \frac{\exp(-\Gamma_{mq} c)}{q\Gamma_{mq}}$$

$$S_{1q}' = \sum_m {}' \frac{\exp(-\Gamma_{mq} c)}{m\Gamma_{mq}}$$

Note that rapid computational formulas for S_m and S_q' were given in (4) and (5) and that S_{1m} and S_{1q}' are already rapidly converging series as defined in (25). Since Δ is actually an unknown in (25), another equation must be introduced before truncation and inversion of (25) in order to have an equal number of equations and unknowns. Kirchhoff's current law as given by (20) cannot be used because it is already built into (25) and would not provide an independent equation. The following convenient condition can be drived from (21):

$$\frac{1}{2} \left[\left. \frac{\partial I_{xo}}{\partial x} \right|_{x=0^-} + \left. \frac{\partial I_{xo}}{\partial x} \right|_{x=0^+} \right] = \frac{1}{2} \left[\left. \frac{\partial I_{yo}}{\partial y} \right|_{y=0^-} + \left. \frac{\partial I_{yo}}{\partial y} \right|_{y=0^+} \right] \qquad (26)$$

In order to be sure of satisfying all three conditions in (21), without an infinite number of terms, it would be necessary to add additional inverse square terms to the current expressions in (23) which would complicate the coupled equations (25) even further. By substituting (23) into (26) and carrying out the differentiations, we obtain:

$$\frac{-\Delta}{\pi} + \sum_m A_m' (im + i\frac{a}{\lambda}\sin\theta\cos\phi) - \sum_q B_q'(iq - i\frac{a}{\lambda}\sin\theta\sin\phi) = 0 \qquad (27)$$

The truncated set of equations from (25) plus (27) can now be inverted to solve efficiently for A_m', B_m', and Δ.

When the new set of equations is tested for convergence on the case shown in Fig. 2, convergence is obtained for a matrix of order 11×11 ($m,q = -2,...2$). The current waveforms given by (23) are shown in Fig. 4, and they are seen to be essentially the same as those in Fig. 3 without the Gibbs' phenomenon oscillations. Other test cases also show very rapid convergence, and the new set of equations can thus be used to obtain parametric curves without using excessive computer time. In all cases, the energy conservation conditions given by (18) and (19) are found to be well satisfied.

The ϕ dependence of the various transmission coefficients is shown in Fig. 5. Note that the bonded mesh coefficients exhibit almost no ϕ dependence. Also, the cross-polarization is negligible on the scale shown. On the other hand, the unbonded mesh transmission coefficients vary markedly with ϕ and sizeable cross-polarization occurs. These effects are in agreement with both the theory and experiment of Kontorovich et al. *(ref. 11)*.

The reflection coefficients for θ polarization are quite important in ground screen applications, and the wavelength dependence is shown in Fig. 6 for $\phi = 0°$ and $\theta = 70°$. Note the more rapid decrease from unity for the bonded mesh. For other values of ϕ the difference is always less. The reflection coefficient for ϕ polarization is also shown, but it does not depend on the junction bonding for $\phi = 0°$.

We have also compared our solution with Otteni's *(ref. 14)* free-space results in his Fig. 4, and we find that his variation in results for different values of ϕ is not correct. He obtains the ϕ variation because he

24

$a/\lambda = 0.25, \quad c/a = 0.02$

$\phi = 0°, \quad \theta = 70°$
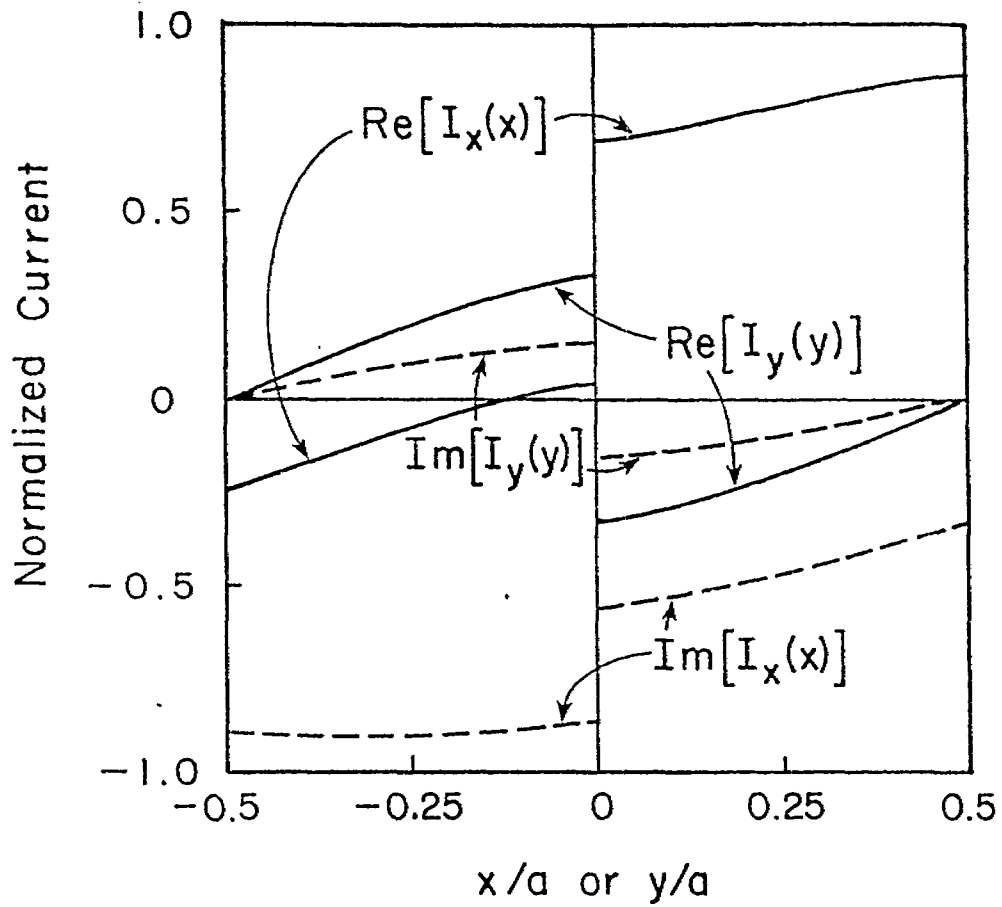
Figure 4

Normalized current waveforms for one Floquet cell as generated by the improved solution.
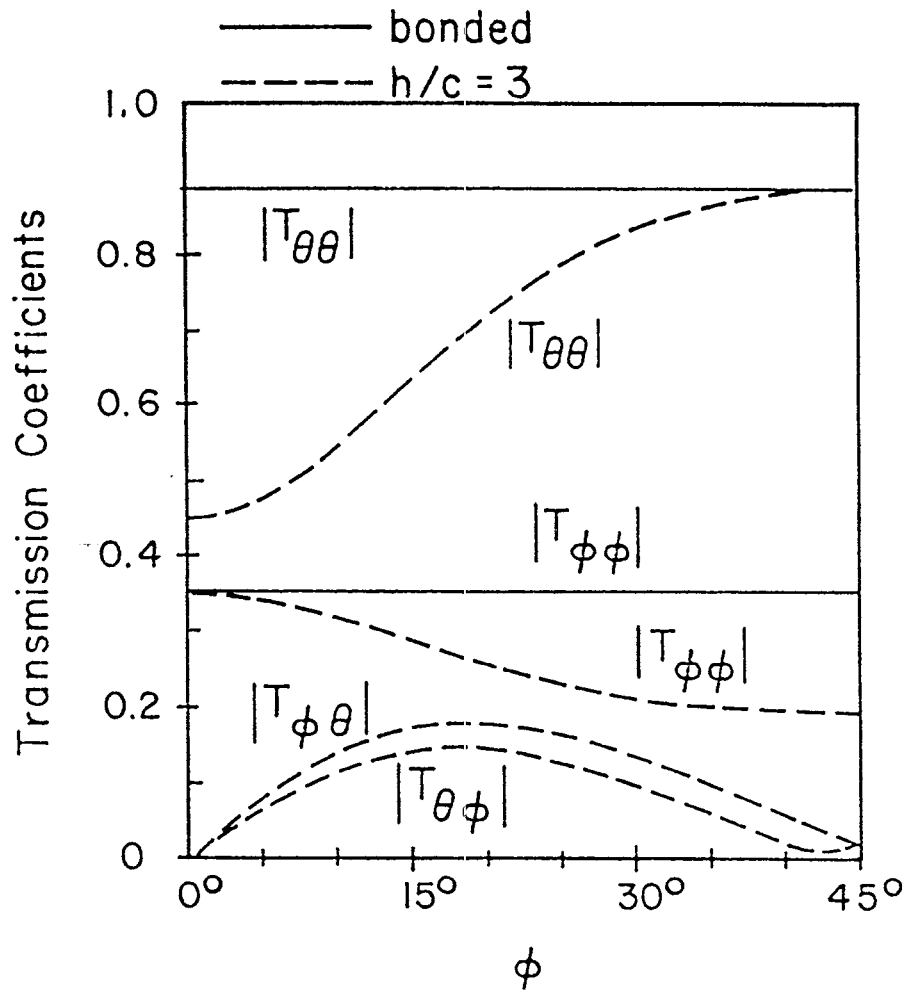
Figure 5   The φ dependence of the various transmission coefficients for bonded and unbonded junctions. $|T_{\theta\phi}|$ and $|T_{\phi\theta}|$ are zero to graphical accuracy for the bonded mesh.
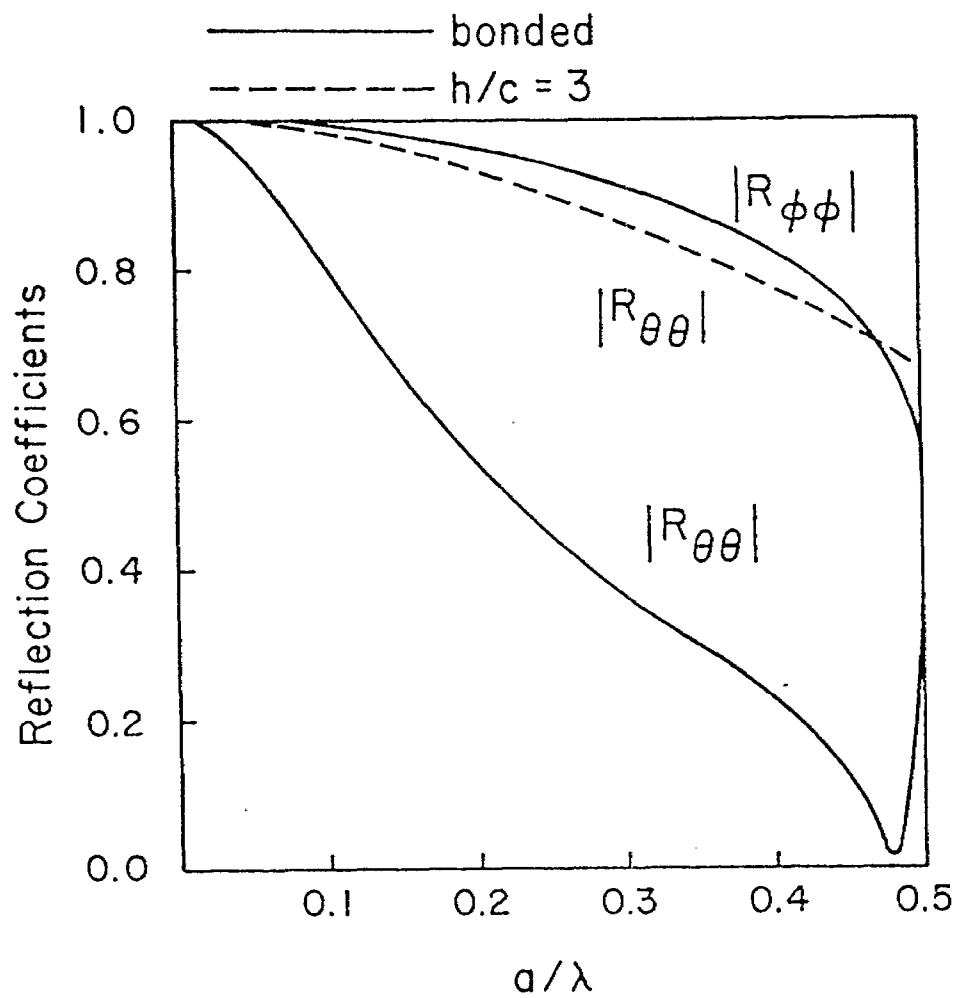
Figure 6 Reflection coefficients for bonded and unbonded junctions. For this case ($\phi=0°$), $|R_{\phi\phi}|$ is independent of the bonding and there is no cross polarization.

has not used enough terms for convergence for small ϕ and θ close to 90° where convergence is extremely slow.

CONCLUDING REMARKS

Plane wave scattering by a bonded mesh has been successfully treated both with and without application of wire junction conditions. However, by building the current jump at the junction into the solution, convergence is greatly improved and computer time is reduced to the point where parametric curves can be easily generated. The same method is applicable to rectangular meshes and imperfectly conducting wires and perhaps to junctions with imperfect contacts since the current jump is obtained directly.

Our results indicate that the properties of a square bonded mesh are essentially independent of ϕ for wire spacings less than a quarter wavelength. Also, for θ polarization, the unbonded mesh provides a larger reflection coefficient (smaller transmission coefficient) for values of ϕ other than 45°. However, the bonded mesh does produce less cross-polarization than the unbonded mesh. Our conclusions are in agreement with Kontorovich et al. *(ref. 11)*, but in disagreement with Otteni *(ref. 14)*.

A worthwhile extension of this analysis would be transient excitation. The rapid computational feature of our improved solution would be useful in generating sufficient frequency domain data for inversion to the time domain. Another useful extension would be to include the influence of a conducting half space whose interface is parallel to the mesh. This configuration has application to antenna ground screens and has been considered for a single wire array parallel to various half-spaces *(refs. 6-10 and 14)*.

28

SECTION III

ELECTROMAGNETIC SURFACE WAVE PROPAGATION
OVER A BONDED WIRE MESH

INTRODUCTION

Wire mesh screens and grids are often employed in electromagnetic shielding devices. They are much cheaper and lighter than sheets of metal but it is important to know what differences can be expected when such structures are used. Using averaged boundary conditions, the reflecting and transmitting properties of crossed wire meshes have been analyzed in the past for both rectangular and square meshes *(refs. 11-13)*. The method appears to give good results for both bonded and unbonded junctions, but is restricted to mesh dimensions small compared with a wavelength. General solutions have also been obtained for plane wave scattering from separated wire grids *(ref. 15)* and bonded wire grids *(ref. 24)*. In general, these solutions require a numerical matrix inversion in solving for the wire currents although perturbation procedures can be used in certain cases.

Here, using a previous formulation *(ref. 24)*, we consider the surface wave that may propagate along a square wire mesh with bonded junctions. Such a surface wave would not be supported by a perfectly conducting surface. This property of wire meshes should be understood when used in any special applications.

Although we consider here a square mesh with perfectly conducting wires, the technique is also applicable to a rectangular mesh with imperfectly conducting wires and in other similar configurations. In the appendix, we discuss the significance of the averaged boundary conditions and an interesting analogy of the wire mesh with a thin plasma sheet.

FORMULATION

The geometry of the bonded mesh in free space (with permittivity ϵ_o and permeability μ_o) is illustrated in Fig. 7. Arrays of wires parallel to the x and y axes with spacing a are centered in the plane $z = 0$, and perfect contacts are made at the junctions. The wire radius c is small compared to both the spacing a and the free space wavelength λ. Consequently, the wires can be considered to carry only axial currents, and thus the usual thin wire approximations are appropriate.

Before proceeding with the analysis, it is worth noting that the mesh structure has a plane of symmetry ($z = 0$). For objects having a plane of symmetry, the electromagnetic field can be decomposed into symmetric and antisymmetric parts which are uncoupled and can be treated separately *(ref. 25)*. The rectangular components of the symmetric part of the electric field satisfy the following:

$$E_{xs}(x,y,z) = E_{xs}(x,y,-z), \quad E_{ys}(x,y,z) = E_{ys}(x,y,-z), \quad \text{and} \quad E_{zs}(x,y,z)$$
$$= -E_{zs}(x,y,-z). \tag{28}$$

The antisymmetric part of the electric field satisfies

$$E_{xa}(x,y,z) = -E_{xa}(x,y,-z), \quad E_{ya}(x,y,z) = -E_{ya}(x,y,-z), \quad \text{and}$$

$$E_{za}(x,y,z) = E_{za}(x,y,-z) \tag{29}$$

Since E_{xa} and E_{ya} are odd in z, they are both zero in the plane of the mesh:

$$E_{xa}(x,y,0) = E_{ya}(x,y,0) = 0 \tag{30}$$

Thus the antisymmetric part of the electromagnetic field does not interact with the mesh (due to the thin wire approximation) and can be treated separately. Here we need consider only the symmetric part of the electromagnetic field and, henceforth, the subscript s is dropped. Also, in
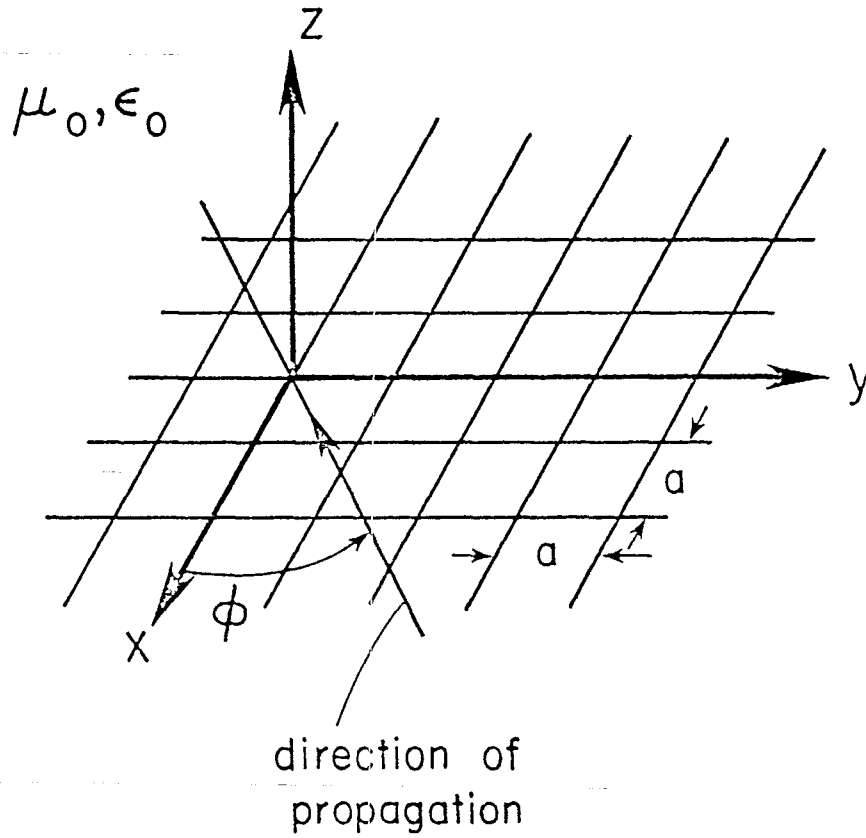
Figure 7   Geometry for a surface wave propagating on a wire mesh with bonded junctions.

what follows, we will assume a time dependence $\exp(i\omega t)$ for all field quantities.

From Floquet's theorem *(ref. 16)*, all electromagnetic quantities can be expressed as an exponential function multiplied by a function which is periodic in x and y. Consequently, if we seek a solution for a surface wave propagating at an angle ϕ to the negative x axis, the current on the qth x-directed wire I_{xq} and the current on the mth y-directed wire I_{ym} can be written:

$$I_{xq} = \exp[\gamma(x \cos\phi + qa \sin\phi)] \sum_{m=-\infty}^{\infty} A_m \exp(i2\pi mx/a) \tag{31}$$

$$I_{ym} = \exp[\gamma(ma \cos\phi + y \sin\phi)] \sum_{q=-\infty}^{\infty} B_q \exp(i2\pi qy/a) \tag{32}$$

Here A_m and B_q are unknown coefficients, and γ is the propagation constant which we seek. The m and q summations indicated in (31) and (32) are over all integers including zero from $-\infty$ to $+\infty$. Because, in general, the currents are discontinuous at the junctions *(ref. 24)*, it is useful to use the equivalent form:

$$I_{xq} = \exp[\gamma(x \cos\phi + qa \sin\phi)]$$

$$\cdot \; [f_\Delta(x) + \sum_m A_m' \exp(i2\pi mx/a)] \tag{33}$$

$$I_{ym} = \exp[\gamma(ma \cos\phi + y \sin\phi)]$$

$$\cdot \; [-f_\Delta(y) + \sum_q B_q' \exp(i2\pi qy/a) \tag{34}$$

where A'_m and B'_q are modified coefficients. The sawtooth function f_Δ has a jump of Δ at the origin and is defined by:

$$f_\Delta(x) = \frac{\Delta}{2\pi i} \sum_n{}' \frac{\exp(i2\pi nx/a)}{n}$$

(35)

$$= \Delta\left[U(x) - \frac{x}{a} - \frac{1}{2}\right], \quad -\frac{a}{2} < x < \frac{a}{2}$$

where
$$U(x) = \begin{cases} 1, & x > 0 \\ 0, & x < 0 \end{cases}$$

The superscripted prime over the summation sign in (35) indicates omission of the $n = 0$ term.

We now invoke the condition that the axial electric fields are zero on the surface of the wires. Because of the thin-wire idealization, we may apply this condition at the tops of the wires. Thus

$$E_x(x,o,c) = E_y(o,y,c) = 0 \tag{36}$$

The expressions for the current in (33) and (34) are identical to those in the case of plane wave scattering *(ref. 24)* except that γ has replaced $ik\sin\theta$ where k was the free space wavenumber $(= 2\pi/\lambda)$ and θ was the angle of incidence. Consequently we need not repeat the derivation. Thus, on omitting the incident field in equation (25) of *ref. 24*, the needed doubly infinite set of equations is found to be:

33

$$- A_m' \left\{ \frac{i\omega\mu_o}{2k^2a} \left[k^2 - \left(\frac{2\pi m}{a} - i\gamma \cos\phi \right)^2 \right] S_m \right\}$$

$$+ \frac{i\omega\mu_o}{2k^2a} \left(\frac{2\pi m}{a} - i\gamma \cos\phi \right) \sum_q B_q' \left(\frac{2\pi q}{a} - i\gamma \sin\phi \right) \frac{\exp(-\Gamma_{mq}c)}{\Gamma_{mq}}$$

$$+ \Delta \left\{ \frac{(\delta_{mo} - 1)}{2\pi i m} \left(\frac{i\omega\mu_o}{2k^2a} \right) \left[k^2 - \left(\frac{2\pi m}{a} - i\gamma \cos\phi \right)^2 \right] S_m \right. \tag{37}$$

$$\left. - \frac{i\omega\mu_o}{2k^2a} \left(\frac{2\pi m}{a} - i\gamma \cos\phi \right) \left[\frac{S_m}{ia} - \frac{\gamma \sin\phi}{2\pi} S_{1m} \right] \right\} = 0$$

$$- B_q' \left\{ \frac{i\omega\mu_o}{2k^2a} \left[k^2 - \left(\frac{2\pi q}{a} - i\gamma \sin\phi \right)^2 \right] S_q' \right\}$$

$$+ \frac{i\omega\mu_o}{2k^2a} \left(\frac{2\pi q}{a} - i\gamma \sin\phi \right) \sum_m A_m' \left(\frac{2\pi m}{a} - i\gamma \sin\phi \right) \frac{\exp(-\Gamma_{mq}c)}{\Gamma_{mq}}$$

$$+ \Delta \left\{ \frac{(1 - \delta_{qo})}{2\pi i q} \frac{i\omega\mu_o}{2k^2a} \left[k^2 - \left(\frac{2\pi q}{a} - i\gamma \sin\phi \right)^2 \right] S_q' \right. \tag{38}$$

$$\left. + \frac{i\omega\mu_o}{2k^2a} \left(\frac{2\pi q}{a} - i\gamma \sin\phi \right) \left[\frac{S_q'}{ia} - \frac{\gamma \cos\phi}{2\pi} S_{1q}' \right] \right\} = 0$$

where
$$S_{1m} = \sum_q{}' \frac{\exp(-\Gamma_{mq}c)}{q\Gamma_{mq}} \quad , \quad S_{1q}' = \sum_m{}' \frac{\exp(-\Gamma_{mq}c)}{m\Gamma_{mq}} \tag{39}$$

and
$$\Gamma_{mq} = \left[\left(\frac{2\pi m}{a} - i\gamma \cos\phi \right)^2 + \left(\frac{2\pi q}{a} - i\gamma \sin\phi \right)^2 - k^2 \right]^{\frac{1}{2}} \tag{40}$$

As indicated in the previous analysis of the scattering problem *(ref. 24)*, the summations given by (39) and (40) can be converted to forms that converge rapidly when the ratio c/a is small. Thus, for present purposes, we use

$$S_m = \frac{a}{\pi} \left\{ - \ln \left[1 - \exp \left(\frac{-2\pi c}{a} \right) \right] + \Delta_m \right\} + \frac{\exp(-\Gamma_{mo}c)}{\Gamma_{mo}} \tag{41}$$

34

$$S'_q = \frac{a}{\pi} \left\{ - \ln \left[1 - \exp \left(\frac{-2\pi c}{a} \right) + \delta_q \right] \right\} + \frac{\exp(-\Gamma_{oq} c)}{\Gamma_{oq}} \qquad (42)$$

where
$$\Delta_m = \frac{1}{2} \sum_q{}' \left[\frac{2\pi}{a} \frac{\exp(-\Gamma_{mq} c)}{\Gamma_{mq}} - \frac{\exp(-2\pi |q| c/a)}{|q|} \right] \qquad (43)$$

and
$$\delta_q = \frac{1}{2} \sum_m{}' \left[\frac{2\pi}{a} \frac{\exp(-\Gamma_{mq} c)}{\Gamma_{mq}} - \frac{\exp(-2\pi |m| c/a)}{|m|} \right] \qquad (44)$$

Also, as shown before *(ref. 24)*, a condition on charge continuity is needed to determine the "current discontinuity" Δ at the junctions. This leads to the requirement that

$$- \frac{\Delta}{\pi} + \sum_m A'_m \left(im - \frac{\gamma \cos\phi}{2\pi} \right) - \sum_q B'_q \left(iq + \frac{\gamma \sin\phi}{2\pi} \right) = 0 \qquad (45)$$

The current expansions as given by (33) and (34) are rapidly convergent; thus, the doubly infinite set of equations in (35) can be truncated with m and q ranging from $-N$ to N where N is a fairly small integer. As a result, a set of $T(= 4N + 3)$ linear, homogeneous equations in A'_m, B'_q, and Δ is obtained:

$$
\begin{bmatrix}
T \times T \\
\text{coefficient} \\
\text{matrix}
\end{bmatrix}
\begin{bmatrix}
A'_{-N} \\
\vdots \\
A'_o \\
\vdots \\
A'_N \\
B'_{-N} \\
\vdots \\
B'_o \\
\vdots \\
B'_N \\
\Delta
\end{bmatrix}
=
\begin{bmatrix}
0 \\
\vdots \\
\vdots \\
\vdots \\
\vdots \\
\vdots \\
\vdots \\
\vdots \\
\vdots \\
\vdots \\
0
\end{bmatrix}
\qquad (46)
$$

A solution to (46) exists only if the determinant, which is a function of γ, vanishes. Symbolically, this is written

$$\det = 0 \tag{47}$$

which is the mode equation to be solved for γ. The resulting z dependence of the associated Floquet harmonics are then given by the factor $\exp(-\Gamma_{mq}|z|)$. For sufficiently small a/λ, there are no grating lobes (Γ_{mq} real) and thus no loss mechanism. Consequently, γ is purely imaginary. The same conclusion can be reached by examining the coefficients in (37), (38), and (45). We might also anticipate that the dominant surface wave mode will have a solution γ near the propagation constant ik of free space.

For small a/λ and large $|z|$, the z dependence is essentially determined by the lowest order Floquet harmonic:

$$\exp(-\Gamma_{oo}|z|) = \exp\left\{-k\left[\left(\frac{\gamma}{ik}\right)^2 - 1\right]^{\frac{1}{2}}|z|\right\} \tag{48}$$

However, as a/λ is increased, grating lobes eventually occur and γ becomes complex. For example, if $\phi = 0°$, the first grating lobe occurs when $\Gamma_{-1,0}$ becomes zero:

$$0 = \Gamma_{-1,0} = \frac{2\pi}{a}\left[\left(-1 + \frac{\gamma}{ik}\frac{a}{\lambda}\right)^2 - \left(\frac{a}{\lambda}\right)^2\right] \tag{49}$$

or

$$\frac{a}{\lambda} = \frac{1}{1 + (\gamma/ik)} \tag{50}$$

Since (γ/ik) actually depends on a/λ, (50) is not an explicit expression for a/λ. Actually, the numerical results in the following section are presented only for the range where a/λ is sufficiently small that γ is purely imaginary.

36

NUMERICAL RESULTS

The mode equation (47) was solved numerically by the bisection method (ref. 26), and the convergence was examined by increasing N until the value of γ did not change significantly. It was found that γ remained essentially constant beyond $N = 2(T = 11)$ which is consistent with the plane wave scattering case (ref. 24). For comparison, approximate results have also been derived from the work of Kontorovich et al (ref. 11)(e.g. see (55) in Section III A.

Results for the relative change in γ for a fairly sparse mesh ($a/c = 500$) are shown in Fig. 8. Note that for small a/λ, the numerical results agree with the approximate soluton and are independent of ϕ. Such behavior is again consistent with the plane wave scattering case (ref. 24). Results for a more dense mesh ($a/c = 50$) are shown in Fig. 9, and the trends are similar, but the relative change in γ is less. In both figures the range of a/λ extends almost to the point where the first grating lobe occurs for $\phi = 0°$. For other ϕ, the first grating lobe occurs at a larger value of a/λ. Of course we need only show ϕ from $0°$ to $45°$ because of symmetry.

PHYSICAL SIGNIFICANCE OF RESULTS

A somewhat crude interpretation of the significance of $(\gamma/ik) - 1$ is as follows. If we wish to propagate a wave on one side of the mesh (such as in antenna ground screens or in parallel plate regions), then the total field must be made up of both a symmetric and an antisymmetric part in order to cancel on one side. Since the propagation constant of the antisymmetric part is that of free space (ik), the phase difference between the symmetric and antisymmetric parts, $\psi_s - \psi_a$, after having propagated
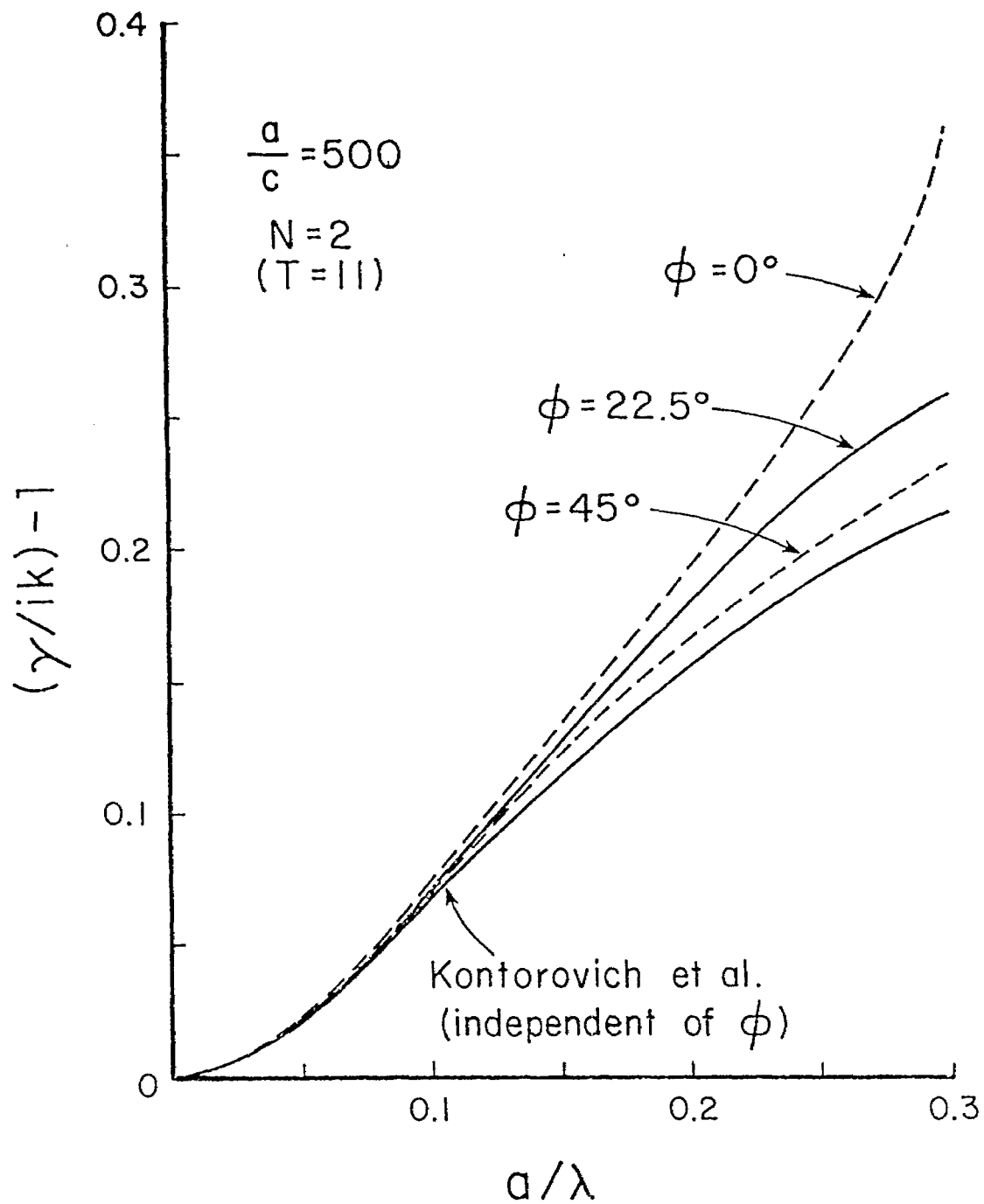
Figure 8   Propagation constant for a sparse mesh as a function of a/λ   for various propagation directions. (Ref. 11)
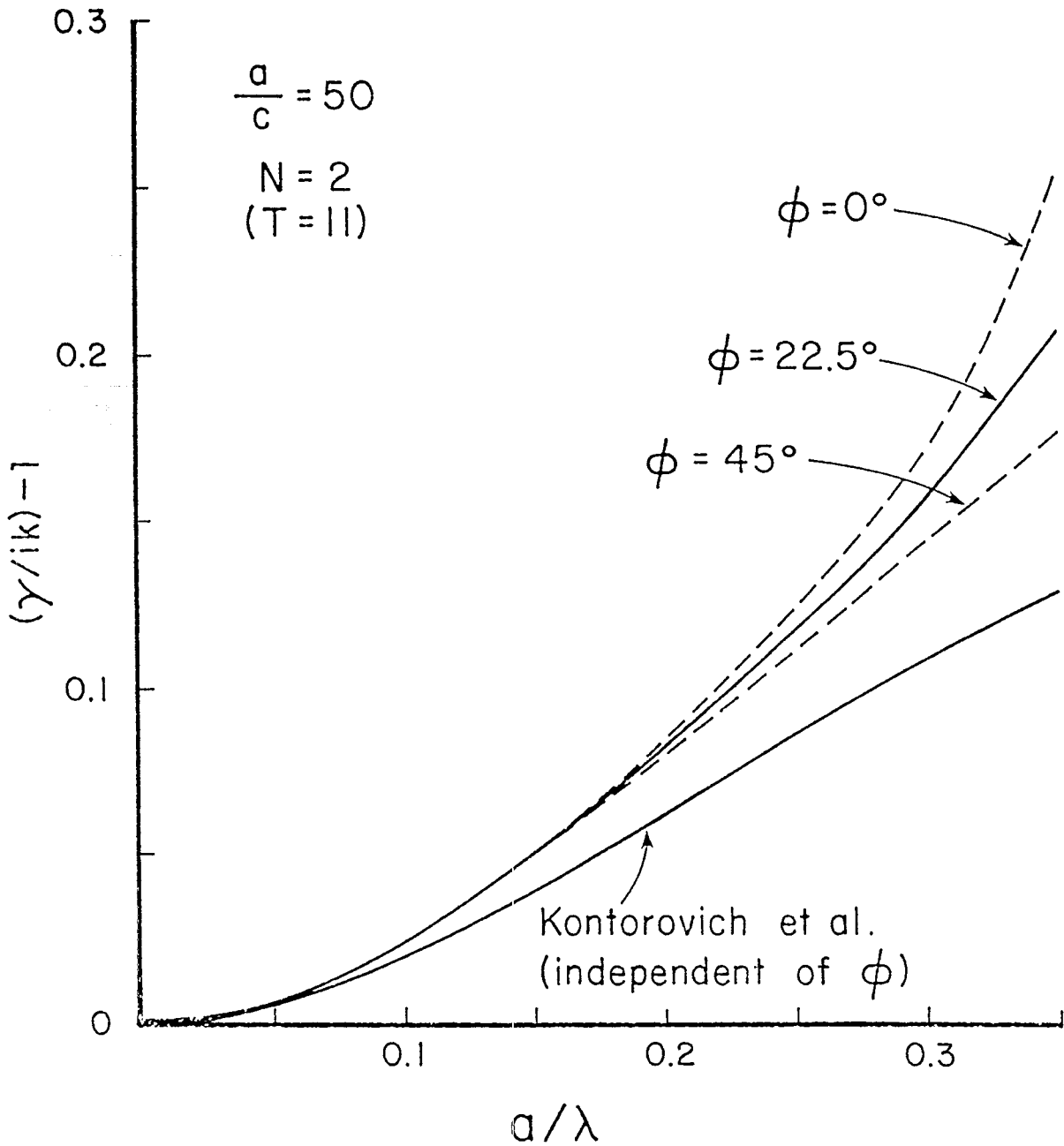
Figure 9 Propagation constant for a more dense mesh. (Ref. 11).

a distance d along the mesh is

$$\psi_s - \psi_a = (\gamma/i)d - kd = kd[(\gamma/ik) - 1] \tag{51}$$

When this phase difference becomes approximately $\pi/2$, the cancellation no longer occurs and the mesh is no longer effective as an electromagnetic shield. In pulse propagation, this phase difference is greatest at the highest frequency component so that the leading edge of the transmitter signal would be most seriously affected. This is just one aspect of the present study that could be followed up with this type of wire mesh model.

CONCLUDING REMARKS

The propagation constant of a surface wave propagating along a square wire mesh in free space has been determined numerically and compared with the approximate solution from the method of averaged boundary conditions. For small mesh spacings, the solutions agree and the results are independent of the direction of propagation. For larger mesh spacings, the propagation constant depends on the direction of propagation as illustrated in Figs. 8 and 9.

A worthwhile extension to this analysis is for imperfectly conducting wires using an impedance boundary condition at the wire surface rather than (36). This does not complicate the formulation, but the propagation constant γ becomes complex. Also, a second mesh (as in a parallel plate waveguide) can be introduced, and this configuration has already been treated by the method of averaged boundary conditions (ref. 27). Finally, the introduction of a lossy half space (ref. 14) would be useful in modelling ground screens for antennas.

40

SECTION III A

AVERAGED BOUNDARY CONDITIONS, THIN PLASMA SHEET ANALOGY, AND EFFECTIVE TRANSFER INDUCTANCE

For a vertically polarized plane wave incident at an angle θ from the z axis, the reflection coefficient R_z as obtained from the method of averaged boundary conditions is *(ref. 11)*

$$R_z = \left[1 + \frac{\alpha k}{\cos\theta}\left(1 - \frac{1}{2}\sin^2\theta\right)\right]^{-1} \tag{52}$$

where

$$\alpha = \frac{ia}{\pi}\ln\left(\frac{a}{2\pi c}\right) \tag{53}$$

As indicated, R_z is normalized so that it would be +1 in the limit of zero grid spacing (i.e. the perfectly conducting plane).

The propagation constant $(\gamma = ik\sin\theta)$ of the surface wave can be determined from the pole location of R_z in the complex θ plane. Thus, the mode equation is:

$$0 = R_z^{-1} = 1 + \frac{\alpha k\left(1 - \frac{1}{2}\sin^2\theta\right)}{[1 - \sin^2\theta]^{\frac{1}{2}}} \tag{54}$$

By substituting $-\gamma^2/k^2$ for $\sin^2\theta$ in (54) and using the quadratic formula, the desired root for γ is found to be

$$\gamma = ik\left\{\frac{(k\alpha)^2 - 1 + [1 - (k\alpha)^2]^{\frac{1}{2}}}{(k\alpha)^2/2}\right\}^{\frac{1}{2}} \tag{55}$$

It is easy to show that the other root of (54) does not satisfy the condition $\text{Im}\cos\theta < 1$ required for fields evanescent in the $\pm z$ direction. For $|k\alpha| \ll 1$, (55) reduces to

$$\gamma \simeq ik \left[1 - \frac{(k\alpha)^2}{8} \right] \simeq ik \left[1 + \frac{1}{8} \left[\frac{ka}{\pi} \ell n \frac{a}{2\pi c} \right]^2 \right] \tag{56}$$

There is an interesting analogy of this wire mesh problem to the situation of a thin plasma sheet that can also support a surface wave. The plasma configurations analyzed earlier *(refs. 28 and 29)* were, in effect, continuous thin slabs of relatively high admittivity so that the induced currents were only in the horizontal plane (i.e. $z = 0$ in the present context). While these earlier analyses dealt with anisotropy resulting from a D.C. magnetic field, we consider here the relevant aspects for the isotropic limit (i.e. gyro-frequency is zero). Thus the thin sheet boundary condition used in *(refs. 28 and 29)* has the form

$$[H_{1y} - H_{2y}] = -ME_x \tag{57}$$

and

$$[H_{1x} - H_{2x}] = ME_y \tag{58}$$

where the subscript 1 denotes the region above the sheet and subscript 2 denotes the region below. The parameter M can be expressed in terms of the sheet thickness δ, plasma frequency ω_o and the collision frequency ν by

$$M = \varepsilon_o \omega_o^2 \delta / (\nu + i\omega) \text{ mhos} \tag{59}$$

If we write

$$M = (r + i\omega\ell)^{-1} \tag{60}$$

we can interpret $r + i\omega\ell$ as the effective transfer impedance of the thin sheet. We note that in the limit of vanishing collision frequency, only the inductive term $i\omega\ell$ survives.

42

Using the results from references 28 and 29, we can write down an expression for the reflection coefficient that is analogous to (52). It is simply

$$R_z = \eta M \cos\theta / (\eta M \cos\theta + 2) \tag{61}$$

where $\eta = (\mu_o / \varepsilon_o)^{\frac{1}{2}}$. The corresponding surface wave pole occurs when $\cos\theta = -2/(\eta M)$ and the corresponding propagation constant is

$$\gamma = + ik \left(1 - \left(\frac{2}{\eta M} \right)^2 \right)^{\frac{1}{2}} \tag{62}$$

$$\simeq ik \left(1 - \frac{2}{(\eta M)^2} \right)$$

in the case where $|\eta M| \gg 1$.

On making a direct comparison of (52) and (61), it is evident that the *effective* value of M, denote M_{eff}, for the wire mesh is given by

$$\eta M_{eff} = \frac{2}{\alpha k [1 - (\sin^2\theta / 2)]} \tag{63}$$

For angles near grazing including the surface wave case thus can be approximated by

$$\eta M_{eff} \simeq 4/(\alpha k) \tag{64}$$

The corresponding expression for effective transfer inductance of the square mesh is

$$\ell_{eff} \simeq \frac{\mu_o a}{4\pi} \ln \frac{a}{2\pi c} \text{ henries} \tag{65}$$

This value for ℓ_{eff} is just one-half for the effective inductance of the wire mesh observed for normal incidence (i.e. $\theta = 0°$). This statement is consistent with the analysis *(ref. 5)* of a parallel grid of spacing a when the electric field is parallel to the wires.

43

It is important to point out that, at normal incidence from a square
mesh, it would not make any difference whether the wire junctions were
bonded or not. However, for oblique incidence and particularly for the
case near grazing, it makes a vast difference unless, of course, $\phi \sim 45°$.
For example, the effective value of the transfer inductance ℓ_{eff} for an
unbonded square mesh at grazing incidence is orders of magnitude smaller
according to the general analysis given in (ref. 24). This statement is also
consistent with the Soviet work (refs. 11-13) but it is in conflict with the
conclusions of Otteni (ref. 14) for reasons we have already discussed (ref.
24).

SECTION IV

ELECTROMAGNETIC SCATTERING BY TWO PERPENDICULAR
WIRE GRIDS OVER A CONDUCTING HALF-SPACE

INTRODUCTION

In an earlier paper (ref.15) an analysis was presented for the scattering of a plane wave by two nonintersecting perpendicular wire grids located in free space. A doubly infinite set of linear equations was derived for determining the coefficients of the doubly harmonic expansions for the currents on the grid wires. These equations were solved by a perturbation procedure that is valid for a reasonably large separation of the grids. In other cases the infinite set was truncated and the solution was obtained by matrix inversion. In a later paper (ref. 24), the limit of zero separation of the perpendicular grids was considered. There it was shown that such mesh structures with bonded wire intersections have vastly different scattering characteristics than for corresponding meshes with un-bonded intersections. It seems significant that the scattering properties determined by the matrix inversion method for both the bonded and unbonded meshes were fully consistent with the theoretical and experimental data published by Kontorovich et al. (ref. 11). They used an approximate analytical method that is valid for small wire spacing.

Here we wish to extend our analysis to the case where the perpendicular grids are located over a conducting half-space. This may be considered as a model to study the screening influence of a wire mesh located over the surface of the earth for an electromagnetic wave incident from above. Such a problem was considered by Otteni (ref. 14) who claimed to have obtained a valid solution for a bonded wire mesh located over the half-space. However, his results are inconsistent with both the data of Kontorovich et al. (ref. 11)

and Astrakhan (ref. 12) as well as the recent analysis by Hill and Wait (ref. 24). The possible reasons for the discrepancies are discussed in the latter reference. In the present formulation we consider explicitly only the unbonded case where the grid wires are nonintersecting . The matrix inversion method in this case is straight-forward and no auxiliary circuit relations need be invoked.

FORMULATION

The situation to be analyzed is illustrated in Fig. 10 with respect to Cartesian coordinates (x,y,z). An array of x-directed thin wires with spacing b is located in the plane $z = 0$. A second array of y-directed wires with spacing a is located in the plane $z = -h$. The common wire radius c is small compared with both the spacings a and b as well as the free space wavelength λ. Consequently, we may assume that the grid wires carry axial currents and, to within a very good approximation, these currents are azimuthally symmetric about the wire axes. The impedance per unit length of the wires is denoted Z_a and Z_b that have dimensions of ohms per unit length. The required impedance boundary conditions are discussed explicitly below.

The region $z > -d$, external to the grid wires, is free space with permittivity ε_o and permeability μ_o. The region $z < -d$ is taken to be homogeneous with permittivity ε_g, conductivity σ_g, and free space permeability μ_o. In the formulation given below, the wire grids are located in the free space region which means that $d > h$ and both these quantities are non negative.

46

As indicated in Fig. 10, the incident plane wave has an arbitrary direction and polarization. Its electric field $\vec{E}^{inc}$, for an implied time factor $\exp(i\omega t)$, can be written

$$\vec{E}^{inc} = \vec{E}_0 \exp\{ik[(x\cos\phi + y\sin\phi)S + zC]\} \tag{66}$$

where $k = (\varepsilon_0\mu_0)^{\frac{1}{2}}\omega = 2\pi/\lambda$, $S = \sin\theta$ and $C = \cos\theta$. The objective now is to deduce the fields scattered from the perpendicular grid wires with due account for the conducting half-space. Here we follow the earlier analysis (ref. 15) but make the necessary generalizations in a manner analogous to that used for analyzing single grids in the presence of a half-space (ref. 8). Thus we choose electric and magnetic Hertz vectors $\vec{\Pi}$ and $\vec{\Pi}^*$ with x and y components in the direction of the grid wires. Conceptually this approach somewhat differs from that used by Otteni (ref. 14) who formulated the problem of the bonded mesh over a half-space by using z directed electric and magnetic Hertz vectors.

FIELD REPRESENTATIONS

As before (ref. 15), we assume that the currents on the x and y directed grids have the respective forms

$$I_{xq} = \sum_{m=-\infty}^{+\infty} A_m \exp\{i[2\pi mx/a + kS(x\cos\phi + qb\sin\phi)]\} \tag{67}$$

$$\text{for} \quad q = 0, \pm 1, \pm 2, \pm 3 \ldots$$

and

$$I_{ym} = \sum_{q=-\infty}^{+\infty} B_q \exp\{i[2\pi qy/b + kS(y\sin\phi + ma\cos\phi)]\} \tag{68}$$

$$\text{for} \quad m = 0, \pm 1, \pm 2, \pm 3 \ldots$$

The summations are over all integer values of m and q from $-\infty$ to $+\infty$ including zero. The coefficients A_m and B_q are as yet unknown.

47
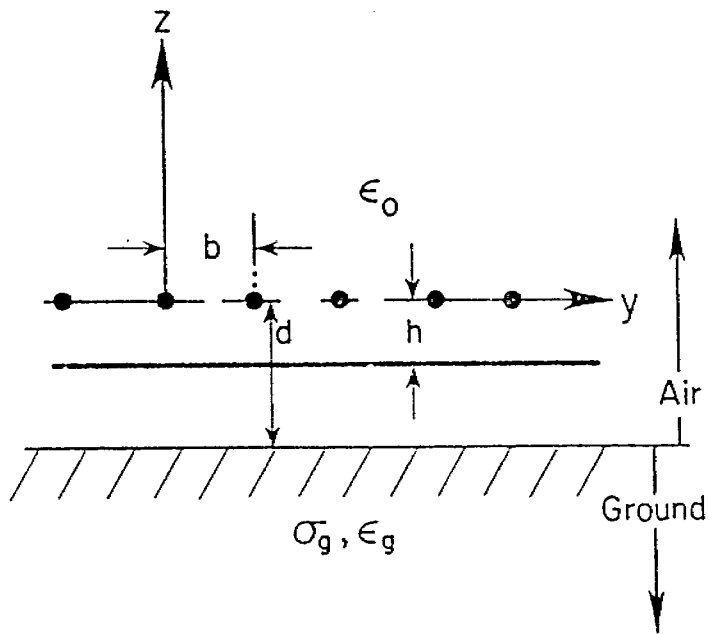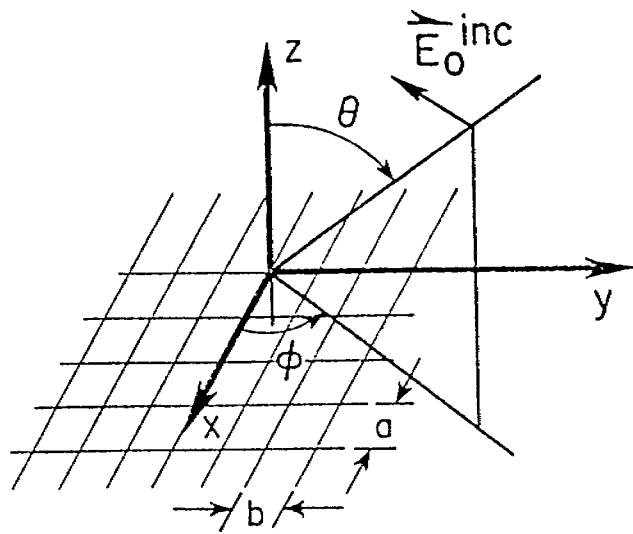
Figure 10   Perpendicular wire grids located over a homogeneous ground or
conducting half-space (perspective and side view).

We are now led to write down, in abbreviated notation, the following representations in the region $z > -d$ for the Hertz potentials due to the grid currents:

$$\Pi_x = - \frac{i\mu_o \omega}{2k^2 b} \sum_m \sum_q A_m [\exp(-\Gamma |z|) + R_{mq} \exp(-\Gamma(z+2d))] \Gamma^{-1} \text{ EXP} \qquad (69)$$

$$\Pi_y = - \frac{i\mu_o \omega}{2k^2 a} \sum_m \sum_q B_q [\exp(-\Gamma |z+h|) + r_{mq} \exp(-\Gamma(z+2d-h))] \Gamma^{-1} \text{ EXP} \qquad (70)$$

$$\Pi_x^* = - \frac{i\mu_o \omega}{2k^2 b} \sum_m \sum_q A_m S_{mq} \exp(-\Gamma(z+2d)) \Gamma^{-1} \text{ EXP} \qquad (71)$$

and

$$\Pi_y^* = - \frac{i\mu_o \omega}{2k^2 a} \sum_m \sum_q B_q s_{mq} \exp(-\Gamma(z+2d)) \Gamma^{-1} \text{ EXP} \qquad (72)$$

where

$$\Gamma = i(k^2 - k_x^2 - k_y^2)^{1/2} = (k_x^2 + k_y^2 - k^2)^{1/2}$$

$$k_x = (2\pi m/a) + kS \cos\phi$$

$$k_y = (2\pi q/b) + kS \sin\phi$$

and

$$\text{EXP} = \exp(ik_x x + ik_y y)$$

Similar expressions for these Hertz potentials apply for the region $z < -d$. The z dependence is now according to $\exp(-\hat{\Gamma}(z+d))$ where

$$\hat{\Gamma} = i(k_g^2 - k_x^2 - k_y^2)^{1/2} = (k_x^2 + k_y^2 - k_g^2)^{1/2}$$

where

$$ik_g = [i\mu_o \omega(\sigma_g + i\epsilon_g \omega)]^{1/2}$$

The corresponding fields $\vec{E}^W$ and $\vec{H}^W$, due to the wire grid currents and their interaction with the lower half-space for $z > -d$ are obtained from

$$\vec{E}^W = k^2\vec{\Pi} + \text{grad div } \vec{\Pi} - i\mu_o\omega \text{ curl}\vec{\Pi}^* \tag{73}$$

and

$$\vec{H}^W = k^2\vec{\Pi}^* + \text{grad div } \vec{\Pi}^* + i\varepsilon_o\omega \text{ curl}\vec{\Pi} \tag{74}$$

For the region $z < -d$, we replace k^2 by k_g^2 and $i\varepsilon_o\omega$ by $(\sigma_g+i\varepsilon_g\omega)$ in the above.

The unknown coefficients in (69) to (72) are now obtained by matching the tangential fields E_x^W, E_y^W, H_x^W and H_y^W across the interface at $z = -d$. This rather tedious algebraic process leads to

$$R_{mq} = \frac{k^2(\Gamma + \hat{\Gamma}K_x)(\Gamma - \hat{\Gamma}\varepsilon_r K_x) + (k_x k_y)^2(1 - K_x)^2}{k^2(\Gamma + \hat{\Gamma}K_x)(\Gamma + \hat{\Gamma}\varepsilon_r K_x) - (k_x k_y)^2(1 - K_x)^2} \tag{75}$$

$$S_{mq} = \frac{-2i\varepsilon_o\omega k_x k_y\Gamma}{k^2(\Gamma + \Gamma K_x)(\Gamma + \hat{\Gamma}\varepsilon_r K_x) - (k_x k_y)^2(1 - K_x)^2} \tag{76}$$

$$r_{mq} = \frac{k^2(\Gamma + \hat{\Gamma}K_y)(\Gamma - \hat{\Gamma}\varepsilon_r K_y) + (k_x k_y)^2(1 - K_y)^2}{k^2(\Gamma + \hat{\Gamma}K_y)(\Gamma + \hat{\Gamma}\varepsilon_r K_y) - (k_x k_y)^2(1 - K_y)^2} \tag{77}$$

and

$$s_{mq} = \frac{+2i\varepsilon_o\omega k_x k_y\Gamma}{k^2(\Gamma + \hat{\Gamma}K_y)(\Gamma + \hat{\Gamma}K_g) - (k_x k_y)^2(1 - K_y)^2} \tag{78}$$

where

$$K_x = (k^2 - k_x^2)/(k_g^2 - k_x^2)$$

$$K_g = (k^2 - k_y^2)/(k_g^2 - k_y^2)$$

$$\varepsilon_r = (\sigma_g + i\varepsilon_g\omega)/(i\varepsilon_o\omega)$$

50

We now consider the appropriate forms of the Hertz potentials for the incident and the reflected fields that would exist in the absence of the wire grids. For the region $z > -d$, these have the relatively simple forms

$$\pi_x = \alpha[\exp(\Gamma_o z) + R_{oo}\exp(-\Gamma_o(z+2d))]\text{EXPO} \tag{79}$$

$$\pi_y = \beta[\exp(\Gamma_o z) + r_{oo}\exp(-\Gamma_o(z+2d)]\text{EXPO} \tag{80}$$

$$\pi_x^* = \alpha S_{oo}\exp(-\Gamma_o(z+2d))\text{EXPO} \tag{81}$$

$$\pi_y^* = \beta s_{oo}\exp(-\Gamma_o(z+2d))\text{EXPO} \tag{82}$$

where

$$\Gamma_o = i[k^2 - k_{ox}^2 - k_{oy}^2]^{1/2}$$

$$k_{ox} = kC\cos\phi$$

$$k_{oy} = kS\sin\phi$$

and

$$\text{EXPO} = \exp(ik_{ox}x + ik_{oy}y)$$

The coefficients R_{oo}, r_{oo}, S_{oo} and s_{oo} are given by (75) to (78) for $m = q = 0$. The factors α and β are prescribed by the incident field. For example, it easily follows that

$$E_{ox} = (k^2 - k_{ox}^2)\alpha - k_{ox}k_{oy}\beta \tag{83}$$

and

$$E_{oy} = (k^2 - k_{oy}^2)\beta - k_{ox}k_{oy}\alpha \tag{84}$$

where E_{ox} and E_{oy} are the tangential field components of the incident field at the origin as indicated by (66).

51

APPLICATION OF WIRE BOUNDARY CONDITIONS

We now come to the "piece de resistance" which is the application of the boundary conditions at the wires. These may be written

$$E_x^{total} = I_{xq}Z_a \quad \text{at} \quad y = qb \quad \text{and} \quad z = c \tag{85}$$

and

$$E_y^{total} = I_{ym}Z_b \quad \text{at} \quad x = ma \quad \text{and} \quad z = -h-c \tag{86}$$

It is not difficult to show that because of the postulated forms of the series representations, we need only apply these conditions explicitly at $y = 0$ and $x = 0$ respectively. In terms of the Hertz potentials the boundary conditions are

$$\left. (k^2 + \frac{\partial^2}{\partial x^2})(\Pi_x + \pi_x) + \frac{\partial^2}{\partial x \partial y}(\Pi_y + \pi_y) + i\mu_o\omega \frac{\partial}{\partial z}(\Pi_y^* + \pi_y^*) \right|_{\substack{y=0 \\ z=c}} = I_{xo}Z_a \tag{87}$$

and

$$\left. (k^2 + \frac{\partial^2}{\partial y^2})(\Pi_y + \pi_y) + \frac{\partial^2}{\partial y \partial x}(\Pi_x + \pi_x) - i\mu_o\omega \frac{\partial}{\partial z}(\Pi_x^* + \pi_x^*) \right|_{\substack{x=0 \\ z=-h-c}} = I_{yo}Z_b \tag{88}$$

Using (69) to (72) and (79) to (82), these lead in a straight-forward manner to

$$\delta_{mo}(k^2 - k_{ox}^2)\alpha[\exp(\Gamma_o c) + R_o \exp(-\Gamma_o(2d+c))]$$

$$- \delta_{mo}\beta k_{ox}k_{oy}[\exp(\Gamma_o c) + [r_o + (i\mu_o\omega\Gamma_o s_o/(k_{ox}k_{oy}))]\exp(-\Gamma_o(2d+c))]$$

$$-A_m[Z_a + i\mu_o\omega(k^2 - k_x^2)P_m/(2k^2 b)] \tag{89}$$

$$+ \frac{i\mu_o\omega}{2k^2 a} k_x \sum_q B_q k_y[\exp(-\Gamma(h+c)) + (r_{mq} + \frac{i\mu_o\omega\Gamma s_{mq}}{k_x k_y}) \exp(-\Gamma(2d-h+c))]\Gamma^{-1} = 0$$

52

when

$$P_m = \sum_q \frac{\exp(-\Gamma c) + R_{mq}\exp(-\Gamma(2d+c))}{\Gamma} \tag{90}$$

and

$$\delta_{qo}(k^2 - k_{oy}^2)\beta[\exp(-\Gamma_o(c+h)) + r_o\exp(-\Gamma_o(2d-h-c))]$$

$$-\delta_{qo}\alpha k_{ox}k_{oy}[\exp(-\Gamma_o(c+h)) + [R_o - (i\mu_o\omega\Gamma_o S_o/(k_{ox}k_{oy}))]\exp(-\Gamma(2d-h-c))]$$

$$-B_q[Z_b + i\mu_o\omega(k^2 - k_y^2)Q_q/(2k^2a)] \tag{91}$$

$$+ \frac{i\mu_o\omega}{2k^2b} k_y \sum_m A_m k_x[\exp(-\Gamma(h+c)) + \left(R_{mq} - \frac{i\mu_o\omega\Gamma S_{mq}}{k_x k_y}\right)\exp(-\Gamma(2d-h-c))]\Gamma^{-1} = 0$$

where

$$Q_q = \sum_m \frac{\exp(-\Gamma c) + r_{mq}\exp(-\Gamma(2d-2h+c))}{\Gamma} \tag{92}$$

As indicated before *(refs. 15 and 24)*, the summations indicated by P_m and Q_q are poorly convergent but they can be transformed to more convenient forms by utilizing the identity

$$\sum_1^\infty \frac{\exp(-\gamma m)}{m} = -\ln(1 - e^{-\gamma}) \simeq \ln(1/\gamma) \quad \text{if} \quad \gamma \ll 1.$$

Thus, provided a, b and d >> c, they can be written in the equivalent forms

$$P_m \simeq \frac{b}{\pi} [\ln \frac{b}{2\pi c} + \Delta_m] + \frac{\exp(-\Gamma_{mo}c)}{\Gamma_{mo}} + \sum_q \frac{R_{mq}}{\Gamma_{mq}} \exp(-\Gamma_{mq}(2d+c)) \tag{93}$$

and

$$Q_q \simeq \frac{a}{\pi} [\ln \frac{a}{2\pi c} + \delta_q] + \frac{\exp(-\Gamma_{oq}c)}{\Gamma_{oq}} + \sum_m \frac{r_{mq}}{\Gamma_{mq}} \exp(-\Gamma_{mq}(2d-2h+c)) \tag{94}$$

where

$$\Delta_m = \frac{1}{2} \sum_q{}' \left(\frac{2\pi}{b\Gamma_{mq}}\right) \exp(-\Gamma_{mq}c) - \frac{1}{|q|} \exp(-2|q|\pi c/b) \tag{95}$$

and

53

$$\delta_q = \frac{1}{2} \sum_m ' \left(\frac{2\pi}{a\Gamma_{mq}} \right) \exp(-\Gamma_{mq}c) - \frac{1}{|m|} \exp(-2|m|\pi c/a) \qquad (96)$$

The primes over the latter two summations indicate that the $m=0$ and $q=0$ terms are to be omitted.

SOLUTION OF COUPLED EQUATIONS AND NUMERICAL EXAMPLES

The infinite set of coupled equations (89) and (91) was truncated and solved for the coefficients A_m and B_q by matrix inversion in the manner described by Hill and Wait *(ref. 15)*. The size of the matrix was increased until there was no sensible change in the value of the coefficients A_o and B_o needed to describe the far scattered field in the case where a and $b < \lambda/2$. There was no problem with convergence since the separation distance h between the grids was non zero.

The numerical results for the scattered fields are presented most meaningfully in terms of reflection coefficients referred to the $z = 0$ plane as described previously *(refs. 15 and 24)*. For example, when the polarization of the incident electric vector is in a plane ϕ = constant, the reflection coefficient $R_{\theta\theta}$ for the scattered electric field in this same plane is defined by

$$R_{\theta\theta} = E_\theta^{s+} \exp\{-ik[(x \cos\phi + y \sin\phi)\sin\theta - z \cos\theta]\}/E_{o\theta}$$

where E_θ^{s+} is the θ component of the total scattered electric field for large positive values of z (i.e. $kz \gg 1$) and $E_{o\theta}$ is the θ component of the incident electric vector at the origin. In the vernacular of radio engineering, $R_{\theta\theta}$ would be called the "vertically polarized reflection coefficient ."

54

Some numerical results of the θ dependence for the amplitude and phase of $R_{\theta\theta}$ for a square mesh (a=b) are illustrated in Figs. 11 and 12 for grid spacings of $a/\lambda = 0.05$ and 0.20 respectively. Two values of ϕ are shown, namely $0°$ and $45°$. The other parameters used are $c/a = 0.01$, $h/c = 3.0$, $d/a = 0.1$, $Z_a = Z_b = 0$, and $\epsilon_r = (\sigma_g + i\epsilon_g\omega)/(i\epsilon_o\omega) = 10 - i1.8$ The latter would correspond to a ground conductivity $\sigma_g = 10^{-2}$mhos/m and relative permittivity $\epsilon_g/\epsilon_o = 10$ at a frequency of 100 MHz. For comparison the corresponding results for the same mesh located in free space are also shown in Figs. 11 and 12 (i.e. the limit of $\epsilon_r = 1$). Then, in addition, the reflection coefficient of the ground or half-space by itself is shown for the same value of ϵ_r (i.e. the limit where $c \to 0$).

The results clearly show that, for incidence in the direction of the wires (i.e. $\phi = 0$), the magnitude of the reflection coefficient remains high for both the mesh in free space and located just over the ground or half-space. This is particularly the case for the smaller mesh spacing. The phase angle of the reflection coefficient also remains reasonably small except for angles near grazing. On the other hand, when the incidence is at $45°$ to the grid wires, the magnitude of the reflection coefficient is substantially reduced for oblique angles of incidence although the results at normal incidence are unchanged. The phase shift on reflection is also somewhat larger for $\phi = 45°$ at the oblique angles and it becomes excessive at grazing angles.

The numerical results illustrated in Figs. 11 and 12 for the mesh in free space are fully consistent with the results of Kontorovich et al. (ref. 11) and Astrakhan (ref. 12) for square meshes with unbonded wire intersections. They use the method based on averaged boundary conditions that clearly distinguishes between bonded and unbonded meshes. As indicated in

55
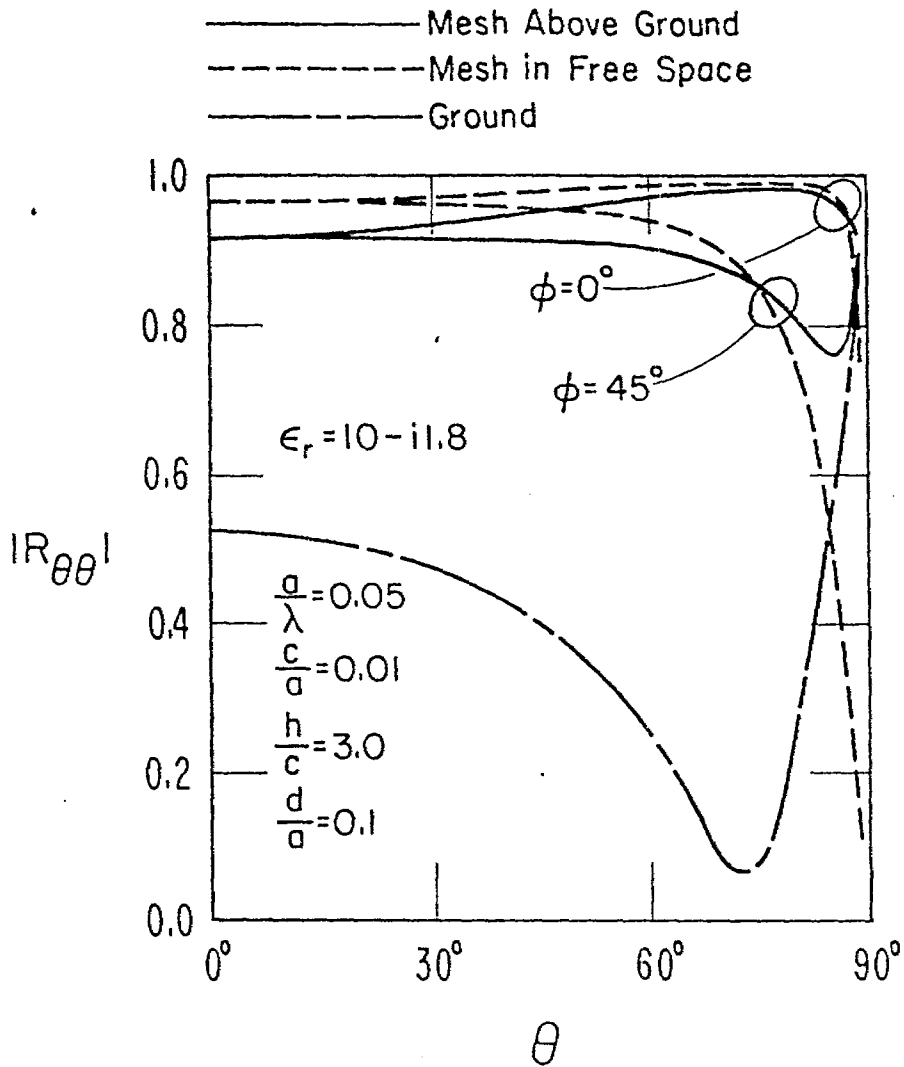
Figure 11a   Amplitude of the reflection coefficient $R_{\theta\theta}$ for $a/\lambda = 0.05$ for mesh over ground and in free space. The corresponding ground reflection in the absence of the mesh is also shown.
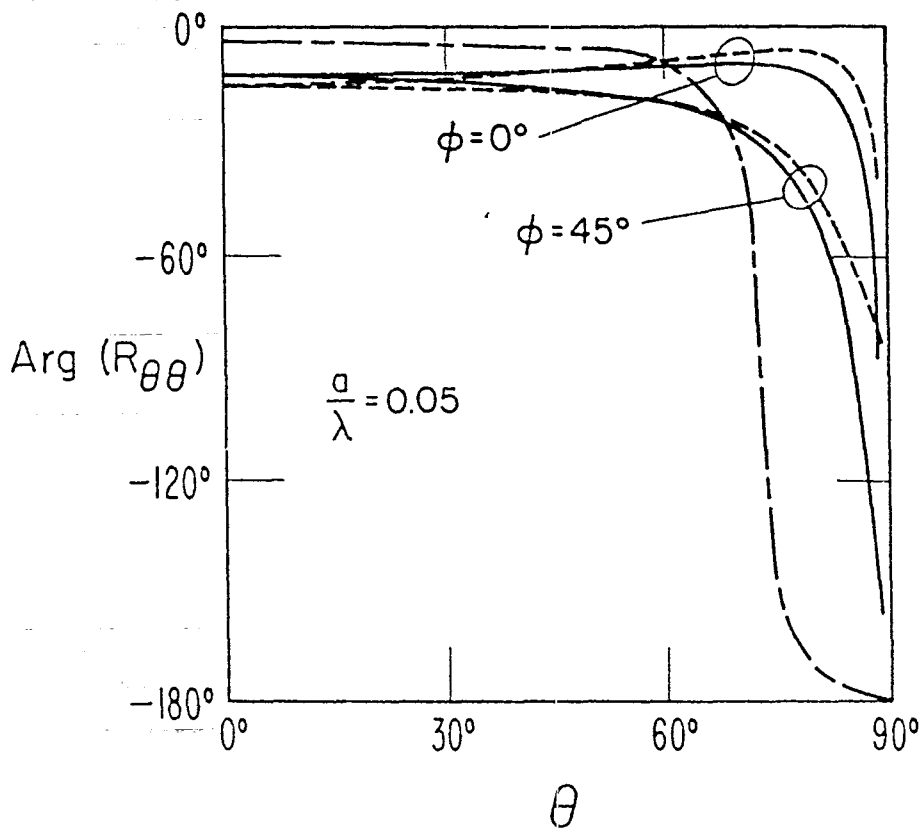
Figure 11b   Phase of the reflection coefficient $R_{\theta\theta}$ for a/λ =0.05 for mesh over ground and in free space. The corresponding ground reflection in the absence of the mesh is also shown.
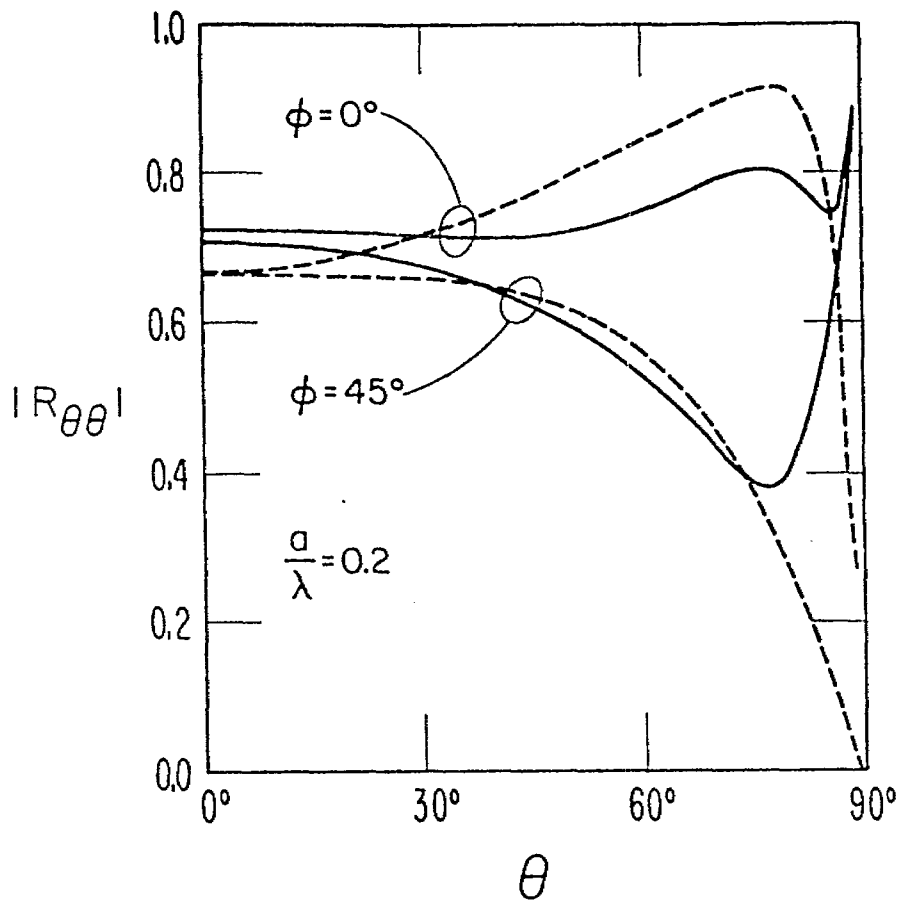
Figure 12a Amplitude of the reflection coefficient $R_{\theta\theta}$ for $a/\lambda = 0.20$
for the mesh over ground and in free space. Conditions are
otherwise the same as for Figure 11.
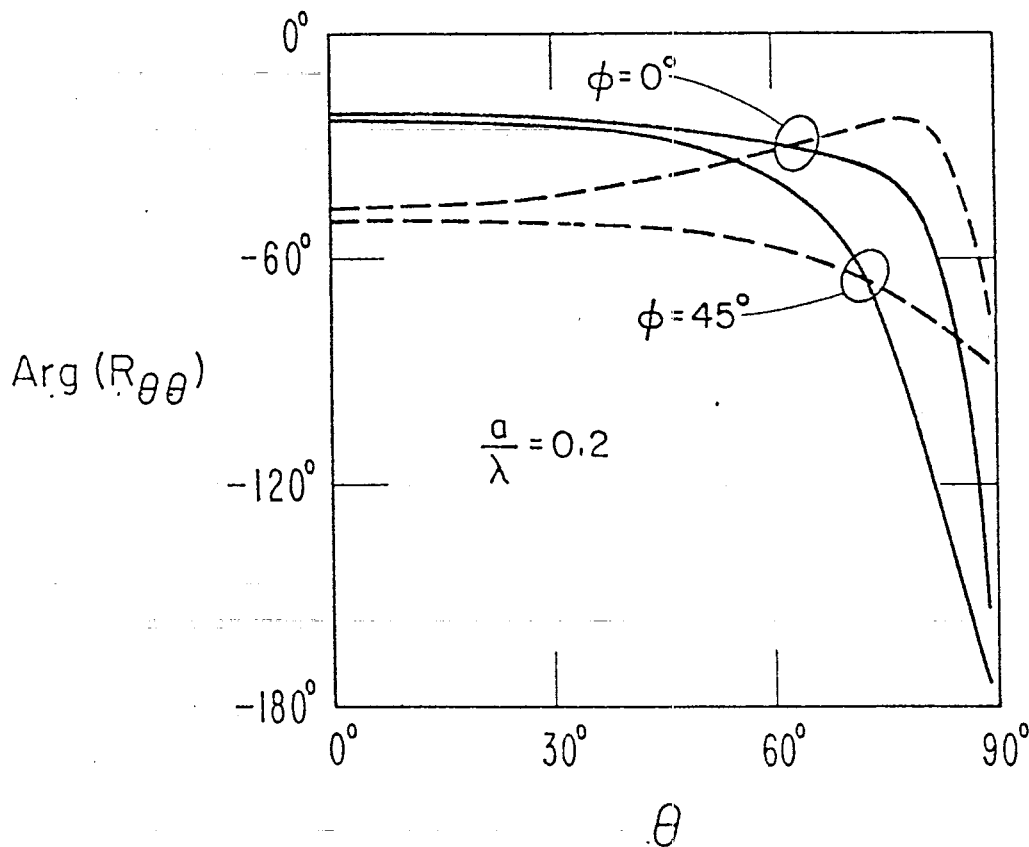
Figure 12b Phase of the reflection coefficient $R_{\theta\theta}$ for a/λ =0.20 for the mesh over ground and in free space. Conditions are otherwise the same as for figure 11.

an earlier paper *(ref. 24)*, we can treat the bonded mesh by the present

boundary value method by allowing h to approach zero. However, in this

case, it is desirable to invoke junction conditions to improve the conver-

gence of the matrix solution of (89) and (91). In the present case, we chose

h = 3c which corresponds to non-intersecting grids in close proximity. In

fact, the results for h in the range h = 2c to 10c or so would not be

sensibly different for the parameters used in Figs. 11 and 12 for all values

of ϕ.

One of the important findings in the earlier studies *(ref. 24)* which

is confirmed by the Soviet work is that bonded and unbonded square.meshes have

identical scattering properties in two special cases. Namely, $R_{\theta\theta}$ is identi-

cal for both bonded and unbonded square meshes if $\phi = 45°$ while $R_{\phi\phi}$

(horizontally polarized reflection coefficient) is identical at $\phi = 0°$.

Also, it was found for meshes with interwire spacings even as large as a quarter

length that the bonded square mesh was essentially isotropic with negligible

cross polarized scattering for all angles ϕ. Thus, we can assert that our

present calculations for $R_{\theta\theta}$ for the unbonded square mesh for $\phi = 45°$

apply to a bonded square mesh for all angles of ϕ. At least this is correct

to within graphical accuracy for the range of parameters employed here.

CONCLUDING REMARKS

The fact that unbonded wire meshes used as ground screens have

superior reflecting properties over bonded wire meshes would seem to be a

major factor in the design of antenna systems for high frequency antennas.

To the authors' knowledge, this fact has not been appreciated in the past

by those responsible for designing such installations. Further analytical

and experimental work on this subject is vitally needed.

SECTION V

ELECTROMAGNETIC SCATTERING FROM AN UNBONDED RECTANGULAR
WIRE MESH LOCATED NEAR THE AIR-GROUND INTERFACE

INTRODUCTION

In an earlier paper *(ref. 30)*, we described a formal analysis for plane

wave scattering by perpendicular wire grids located above a conducting half-

space. To illustrate the method, a few numerical examples were presented

for the "vertically polarized reflection coefficient" of a square mesh. However,

there are many parameters that influence the scattered field; thus a numerical

study is needed to gain a proper understanding of the situation. This is the

purpose of the present paper. We also consider the radiation patterns of

short dipoles located above the wire mesh for various conditions.

The situation for plane wave incidence is illustated in Fig. 13. An

array of x-directed wires is located in the plane $z = 0$, and an array of

y-directed wires is located in the plane $z = -h$. The wire radius c is

small compared with both the spacings a and b as well as the free space

wavelength λ. The wires, assumed here to be perfectly conducting, are

immersed in free space with permittivity ε_o and permeability μ_o. The

region $z < -d$ is taken to be homogeneous with permittivity ε_g, con-

ductivity σ_g, and free space permeability μ_o.

As we indicated earlier *(refs. 24 and 30)*, the far field reflecting

properties of the configuration, for both a and b less than $\lambda/2$, are

completely characterized by the four reflection coefficients: $R_{\theta\theta}$, $R_{\theta\phi}$,

$R_{\phi\theta}$, and $R_{\phi\phi}$. The subscript θ refers to the electric field polarized

in the plane of incidence, and the subscript ϕ refers to the electric

field polarized perpendicular to the plane of incidence. The first sub-

script refers to the state of polarization of the incident wave while the
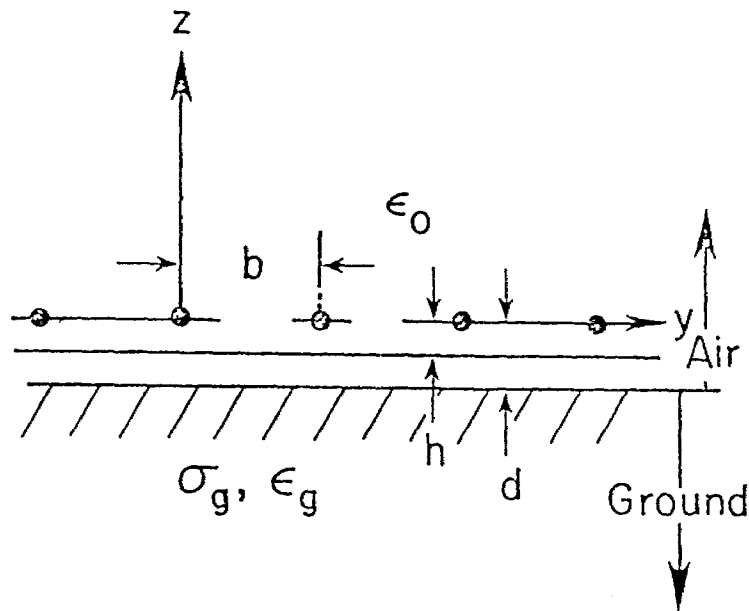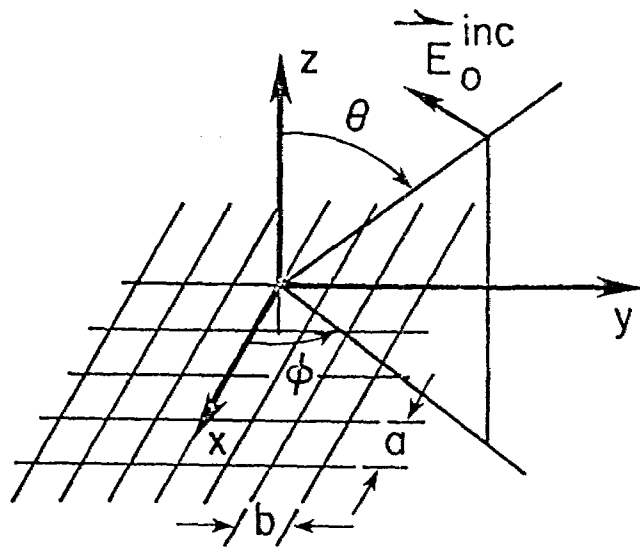
Figure 13   Perpendicular wire grids located over a conducting half-space
              (perspective and side view).

second subscript refers to the reflected wave. Consequently, in radio

engineering terminology, $R_{\theta\theta}$ is the "vertically polarized reflection co-

efficient," $R_{\phi\phi}$ is the "horizontally polarized reflection coefficient",

and $R_{\theta\phi}$ and $R_{\phi\theta}$ are the "cross-polarized reflection coefficients". In

matrix notation the reflection coefficient can be written

$$\begin{vmatrix} R_{\theta\theta} & R_{\theta\phi} \\ R_{\phi\theta} & R_{\phi\phi} \end{vmatrix}$$

EFFECT OF MESH HEIGHT

In the following results, the grid separation h is taken equal to

3c. This separation has been shown to yield results which are representative

of an "unbonded" mesh (ref. 24), but the results are not strongly dependent

on h provided $h > 2c$. Since some wire mesh ground screens are actually

in contact with the earth or even slightly buried, it is desirable to show

some results for a small mesh height d. The separation between the y-

directed wires and the earth is $d - h - c$ which must be positive in this

particular formulation and should be greater than or equal to c to satisfy

the thin wire approximations.

The magnitude and phase of $R_{\theta\theta}$ for $d - h - c$ equal to c and 6c

are illustrated in Figs. 14a and 14b. The other parameters are: $a/\lambda = b/\lambda$

$= 0.05$, $c/a = 0.01$, $h/c = 3.0$, and $\varepsilon_r = (\varepsilon_g - i\sigma_g/\omega)/\varepsilon_0 = 10.0 - i1.8$. The

latter corresponds to a ground conductivity $\sigma_g = 10^{-2}$ mhos/m at a frequency

of 100 MHz. As expected, the reflection coefficient is larger for $\phi = 0°$

than for $\phi = 45°$. Actually, the results for $\phi = 45°$ can be approximately

identified as those for a bonded mesh (h=0) at any value of ϕ since the

bonded mesh is quite isotropic in its ϕ behavior (ref. 30). Also, note
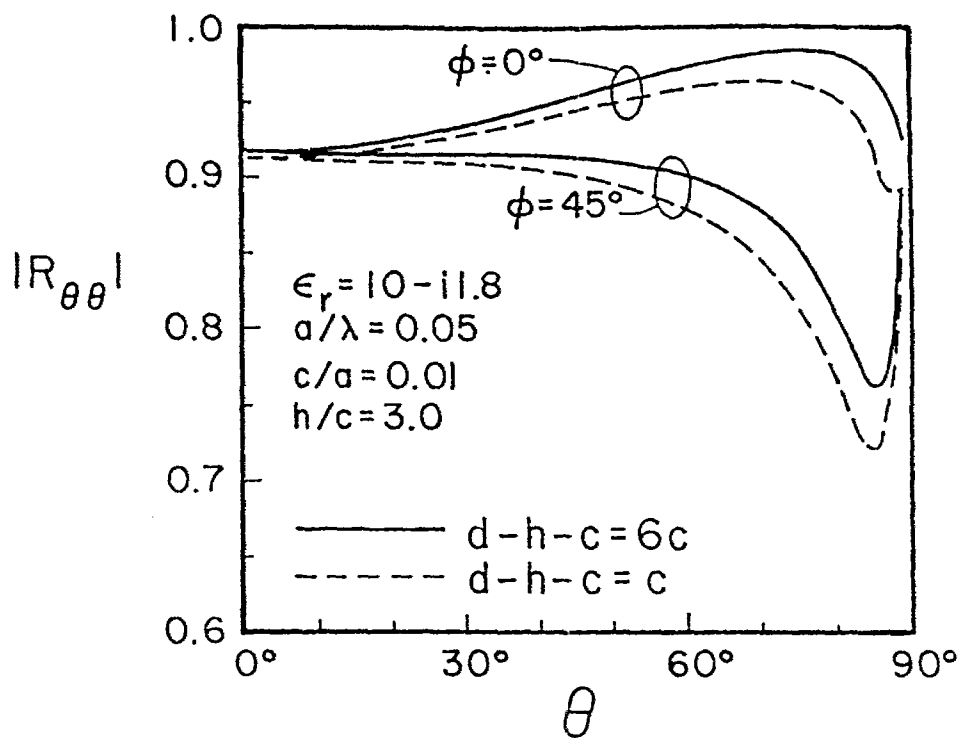
Figure 14a
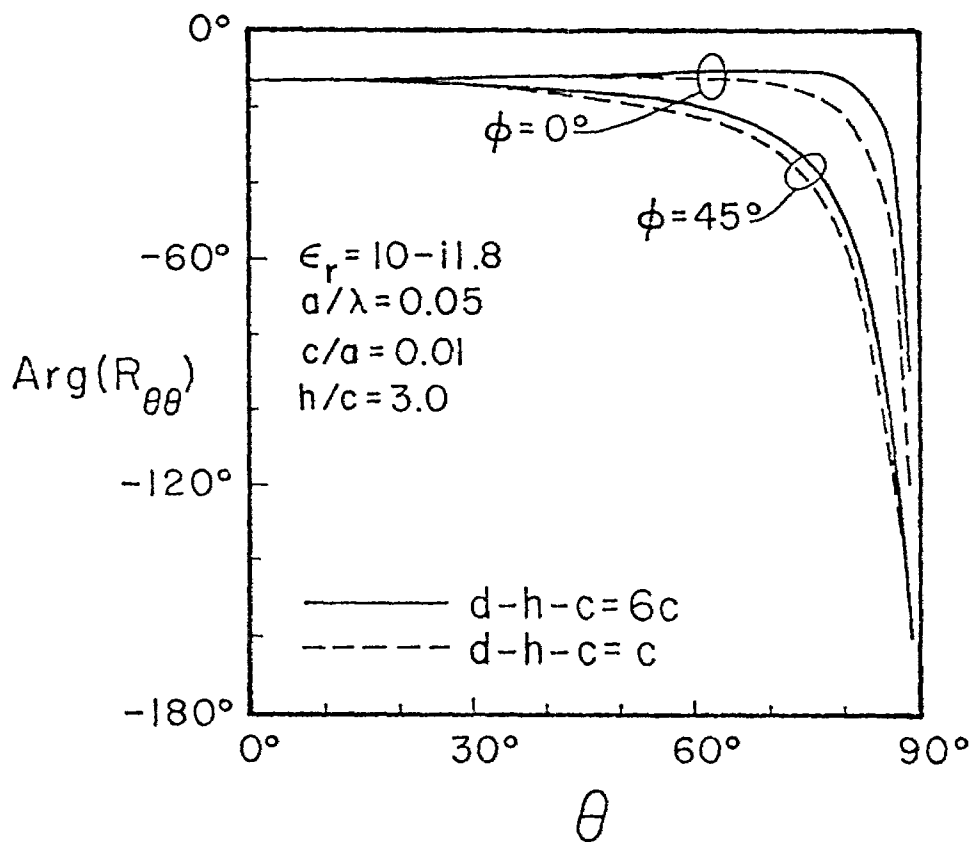
Figure 14b

Figures 14a   Magnitude and phase of the reflection coefficient $R_{\theta\theta}$ for a mesh
  and   14b   at two heights above ground.

that the reflection coefficient magnitude and phase are degraded when the mesh is located close to the earth (d-h-c=c). This behavior is consistent with that of a single wire grid over a half space *(ref. 9)*.

HORIZONTAL POLARIZATION

Although ground screens are more commonly used for vertically polarized radiation, the "horizontally polarized reflection coefficient" $R_{\phi\phi}$ is also of some interest. Thus, we show the behavior of the magnitude of $R_{\phi\phi}$ in Fig. 15 for the same parameters as those in Fig. 14. The departure of $|R_{\phi\phi}|$ from unity is quite small (note the enlarged scale), and again there is a slight degradation when the mesh is closer to the ground (d-h-c=c). Also note that there is little difference between the results for $\phi = 0°$ and $\phi = 45°$.

For $R_{\phi\phi}$, the results are identical for bonded and unbonded meshes at $\phi = 0°$, and the bonded mesh properties again are nearly independent of ϕ. Consequently, for ϕ near 45°, the unbonded mesh is somewhat better (larger $|R_{\phi\phi}|$). The phase is not shown because it is in the vicinity of 180° for all cases.

The cross polarized reflection coefficients, $R_{\theta\phi}$ and $R_{\phi\theta}$, are not shown because they are identically zero at $\phi = 0°$ and very small at $\phi = 45°$. They generally peak at about $\phi = 25°$, but for the small mesh spacing given in Figs. 2 and 3 (a/λ=0.05), they are always small.

RECTANGULAR MESH

Since rectangular meshes (a ≠ b) are often used in practice, it was decided to extend the previous computer program to the case where a ≠ b. Here we compared the predictions based on the approximate average boundary
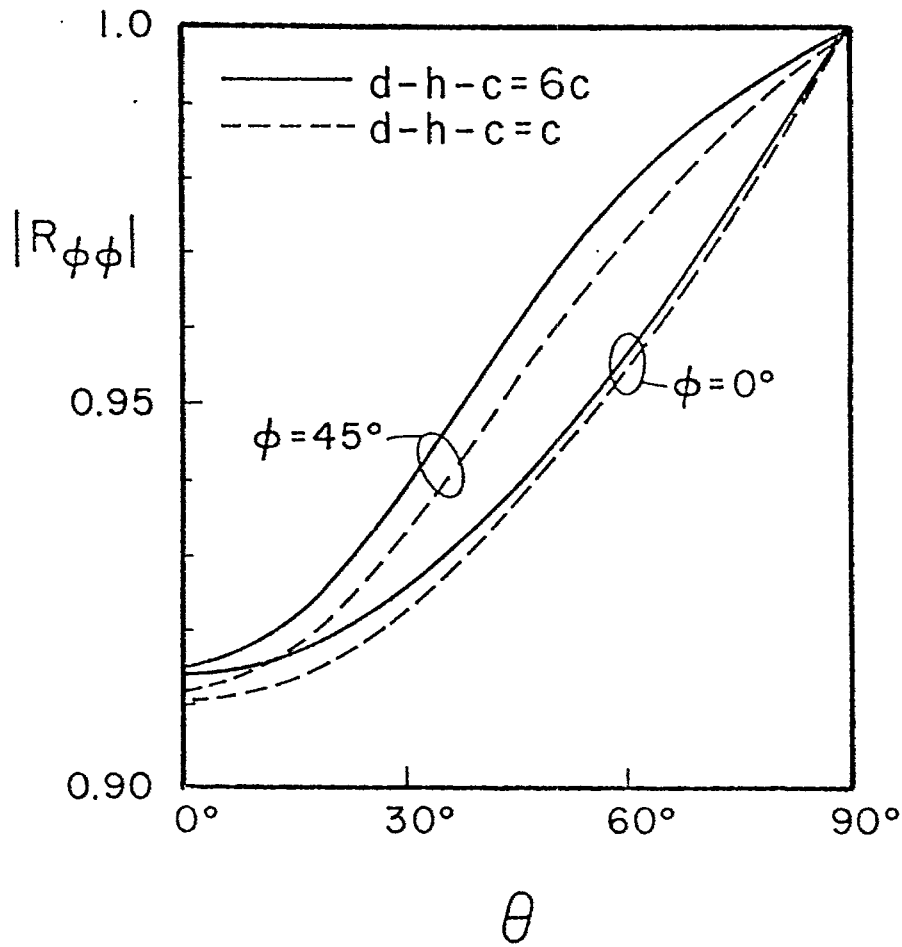
Figure 15 Magnitude of the horizontally polarized reflection coefficient $R_{\phi\phi}$ for the same conditions as Figure 14.

condition. Astrakhan *(ref. 12)* and other Soviet workers have often used the latter approach. To facilitate the comparison, his equations were programmed after correcting his equation 14 ($\gamma_2 \sin^2\phi$ should be $\gamma_1 \sin^2\phi$). Since Astrakhan's results only apply to the free space case, we must set $\varepsilon_g = \varepsilon_o$ and $\sigma_g = 0$ in our formulation. A comparison is shown for four values of ϕ in Figs. 16a-16d for $a/\lambda = 0.2$, $b/\lambda = 0.1$, and $c/\lambda = 2 \times 10^{-3}$. Again we chose $h = 3c$, although this separation parameter does not occur explicitly in the Astrakhan formulation. Here, of course, a 90° range in ϕ is required to cover all cases for the rectangular mesh.

The results for $R_{\phi\theta}$ are not shown because the Astrakhan model predicts $R_{\phi\theta} = -R_{\theta\phi}$ and our model yields $R_{\phi\theta} \simeq -R_{\theta\phi}$. It is significant in Figs. 16b and 16c that the rectangular mesh produces significant cross polarization. The main deviation occurs in $R_{\theta\theta}$ at $\theta = 90°$ for $\phi = 0°$ or 90° where the Astrakhan model predicts $R_{\theta\theta} = 1$ rather than zero. This occurs because the Astrakhan model does not include the effect of the cross wires in this case. The phases are not shown because they are less interesting, but the agreement is similar.

Although the method of average boundary conditions is strictly valid only for a/λ and b/λ small, we show some further results for $a/\lambda = 0.5$, $b/\lambda = 0.25$, and $c/\lambda = 5 \times 10^{-3}$ in Figs. 17a and 17b. Here the agreement is not as good, particularly for $\phi = 0°$ and θ approaching 90° in Fig. 17a. This is because the first grating lobe is ready to emerge as θ approaches 90°.

For the rectangular mesh, the bonded and unbonded meshes no longer yield the same result for $R_{\theta\theta}$ at $\phi = 45°$. Consequently, a useful extension would be to treat the bonded $(h=0)$ rectangular mesh by means of the method
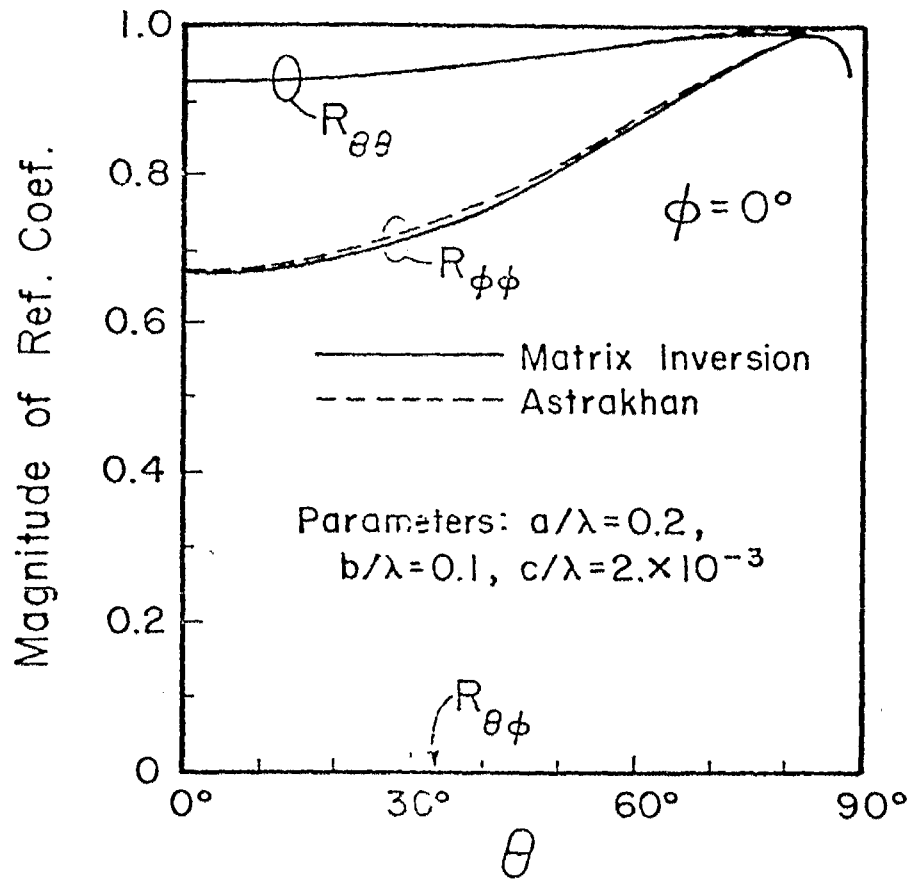
Figure 16a
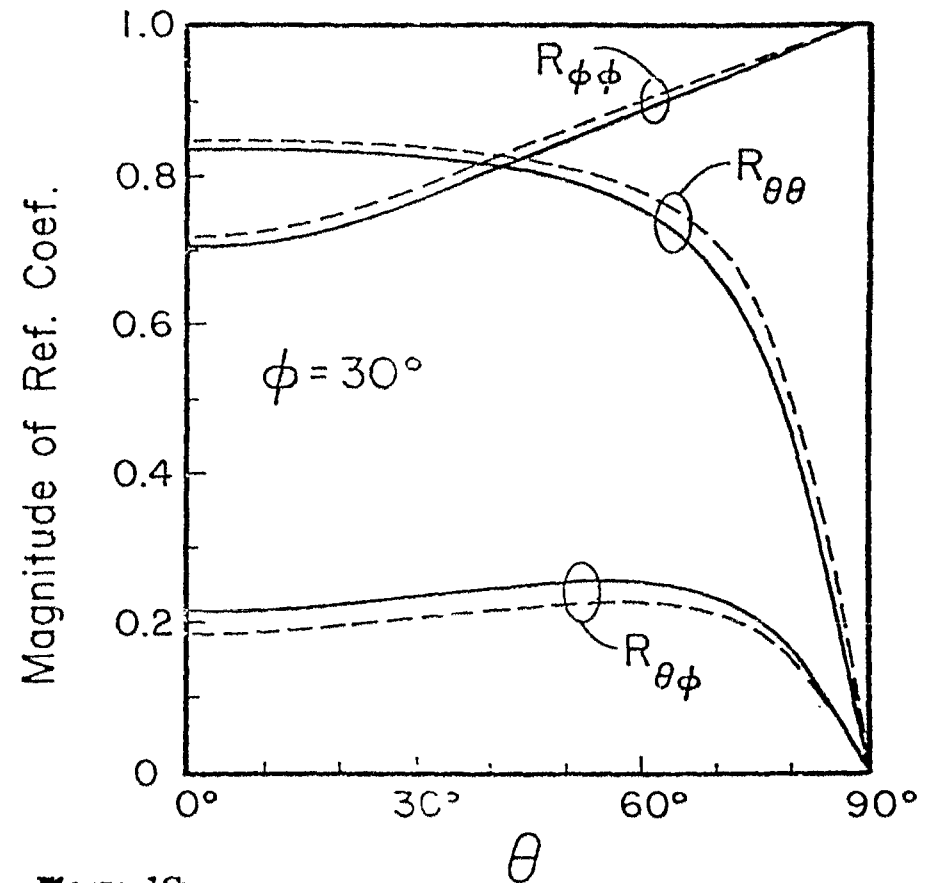
Figure 16b

Figures 16a, 16b, Magnitude of the various reflection coefficients for $\phi = 0°$, 30°
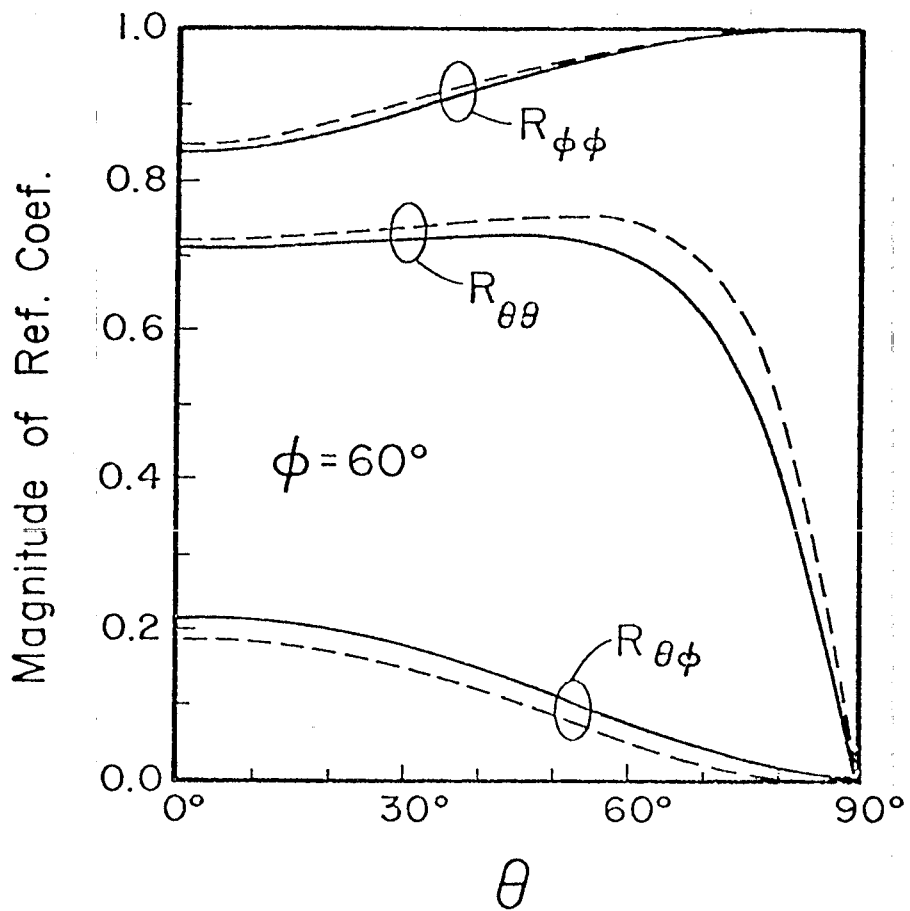
Figure 16c
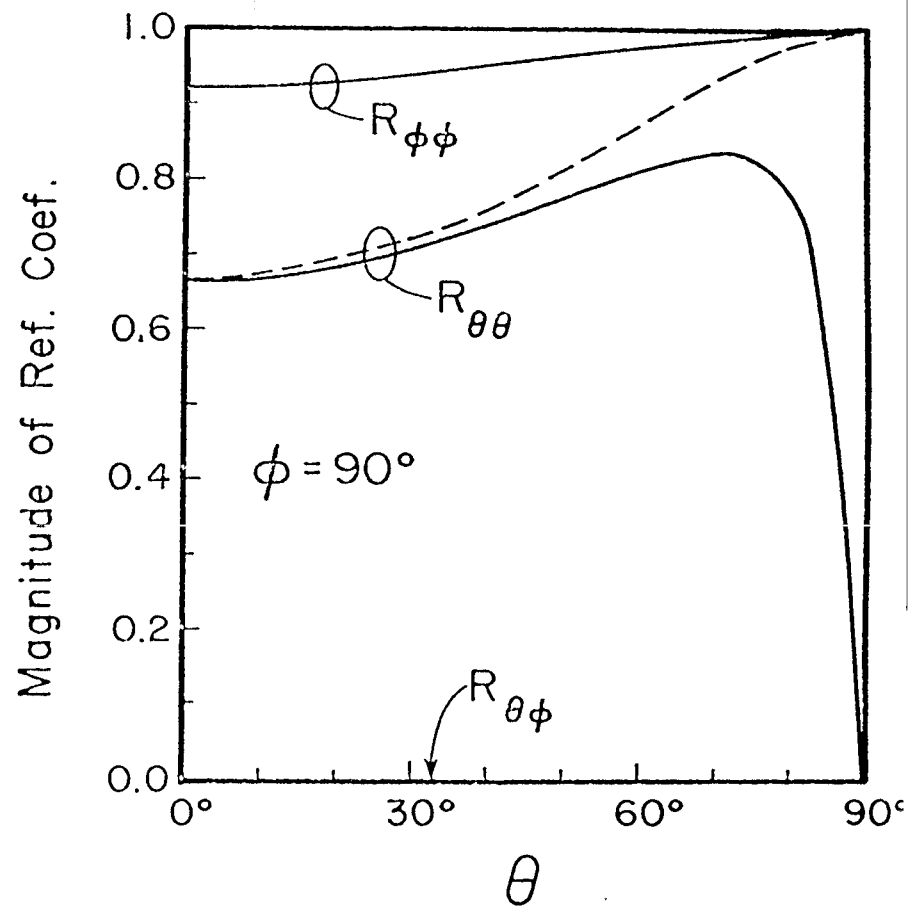
Figure 16d

Figures 16c, 16d, Magnitude of the various reflection coefficients for $\phi = 60^\circ$, 90°

69

Parameters: $a/\lambda = 0.5$, $b/\lambda = 0.25$, $c/\lambda = 5. \times 10^{-3}$

Figure 17a
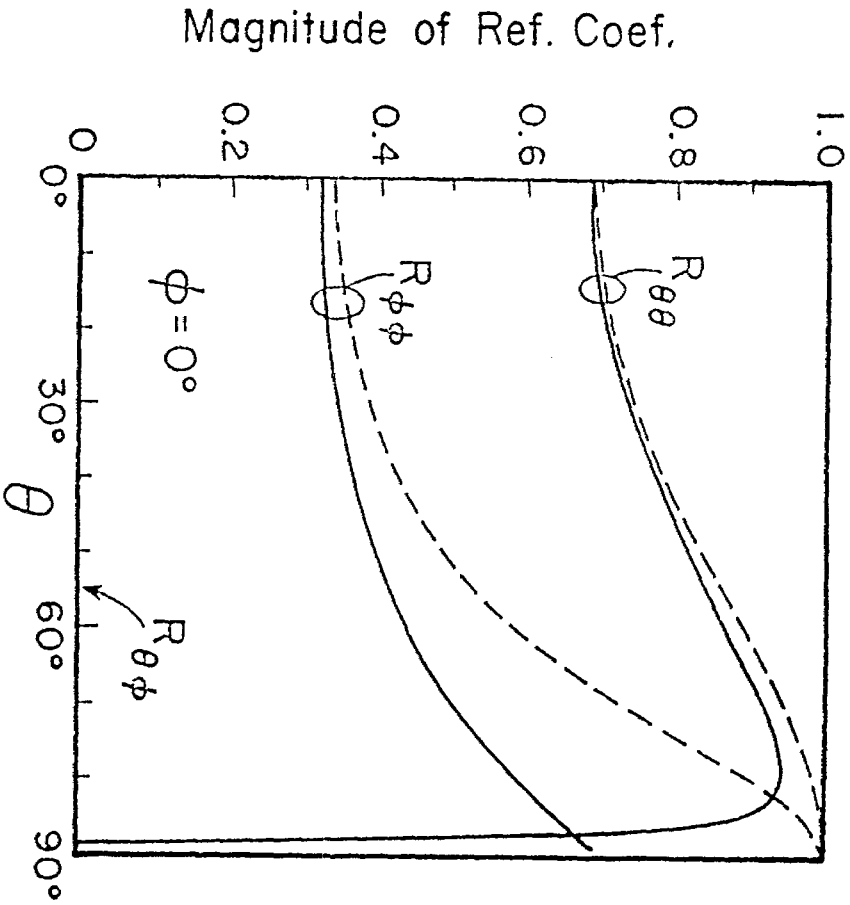
Parameters: $a/\lambda = 0.5$, $b/\lambda = 0.25$, $c/\lambda = 5. \times 10^{-3}$

Figure 17b

Figures 17a   Magnitude of the various reflection coefficients for $\phi = 0$ and 30°
and 17b   for a larger rectangular mesh.
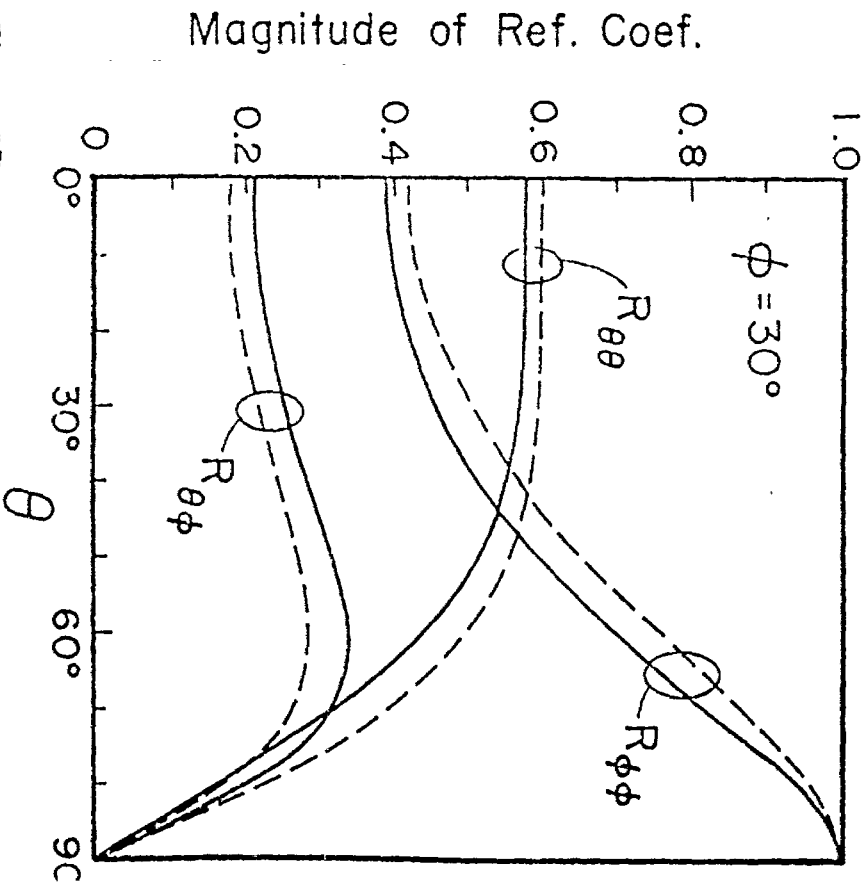
previously employed for the square bonded mesh *(ref. 24).* This remains to be done.

DIPOLE RADIATION PATTERNS

Although the near field of a source dipole above a mesh is quite complex, fairly simple far-field expressions can be derived by reciprocity. Consider a source dipole of moment $Id\ell$ with $\exp(i\omega t)$ time dependence located at $(x,y,z) = (0,0,\ell)$ in the same geometry described in Fig. 13. The far-zone electric field at (r,θ,ϕ) has only θ and ϕ components E_θ and E_ϕ which can be written in the following forms:

$$E_\theta = CP_\theta \quad \text{and} \quad E_\phi = CP_\phi \tag{97}$$

where

$$C = (i\mu_o\omega/4\pi)Id\ell \, \exp[-ik_o(r - \ell \cos\theta)] \tag{98}$$

To cover all possible cases, we derive P_θ and P_ϕ for x-, y- and z-directed dipoles. Results for arbitrary dipole orientation can then be obtained by resolving the dipole moment into x, y, and z components with subsequent superposition of the respective radiation fields. For a z-directed dipole, we have:

$$P_\theta = (1 + R_{\theta\theta}\exp)\sin\theta \tag{99}$$

and

$$P_\phi = (R_{\theta\phi}\exp)\sin\theta \tag{100}$$

where

$$\exp = \exp(-i2k_o\ell \cos\theta)$$

For an x directed dipole,

$$P_\phi = -(1 + R_{\phi\phi}\exp)\sin\phi + (R_{\theta\phi}\exp)\cos\phi \, \cos\theta \tag{101}$$

71

and

$$P_\theta = -(1 - R_{\theta\theta}\exp)\cos\theta\,\cos\phi - (R_{\phi\theta}\exp)\sin\phi \qquad (102)$$

Finally, for a y directed dipole,

$$P_\phi = -(1 + R_{\phi\phi}\exp)\cos\phi + (R_{\theta\phi}\exp)\sin\phi\,\cos\theta \qquad (103)$$

and

$$P_\theta = -(1 - R_{\theta\theta}\exp)\cos\theta\,\sin\phi + (R_{\phi\theta}\exp)\cos\phi \qquad (104)$$

Strictly speaking, the above results are valid only for ℓ somewhat greater than a and b so that the higher order evanescent modes are negligible. However, for small ℓ, these results are still valid if the dipole position is averaged over one mesh cell $(-a/2 < x < a/2$ and $-b/2 < y < b/2)$ since the evanescent fields have a zero average.

To illustrate the radiation patterns, the following parameters are chosen: $a/\lambda = b/\lambda = 0.05$, $c/a = 0.01$, $h/c = 3$, $d/a = 0.1$, and $\epsilon_r = 5.0 - i0.18$. The latter corresponds to a ground conductivity $\sigma_g = 10^{-3}$mho/m at a frequency of 100 MHz. This ϵ_r value was chosen to illustrate the improvement provided by the mesh over poorly conducting ground. Fig. 18 illustrates $|P_\theta|$ for a vertical (z-directed) dipole located at the mesh surface $(\ell=0)$ for three values of ϕ. The patterns for ground alone and for perfect ground alone are also shown, and they are independent of ϕ. Also shown is the cross-polarized pattern, $|P_\phi|$, which is quite small even for $\phi = 22.5°$. It is zero for $\phi = 0°$ and very small for $\phi = 45°$. Fig. 19 illustrates the same case except that the dipole is now elevated $(\ell/\lambda = 0.5)$ so that an extra lobe is introduced into the pattern. Note that "cutback" still occurs as θ approaches 90°.

Mesh Above Ground
Perfect Ground
Ground

$$\epsilon_r = 5 - i0.18$$
$$\frac{a}{\lambda} = 0.05$$
$$\frac{c}{a} = 0.01$$
$$\frac{h}{c} = 3.0$$
$$\frac{d}{a} = 0.1$$
$$\ell = 0$$

$|P_\theta|$

$\phi = 0°$
$22.5°$
$45°$

$|P_\phi|,\ \phi = 22.5°$

2.0
1.5
1.0
0.5
0

0°　　30°　　60°　　90°

θ
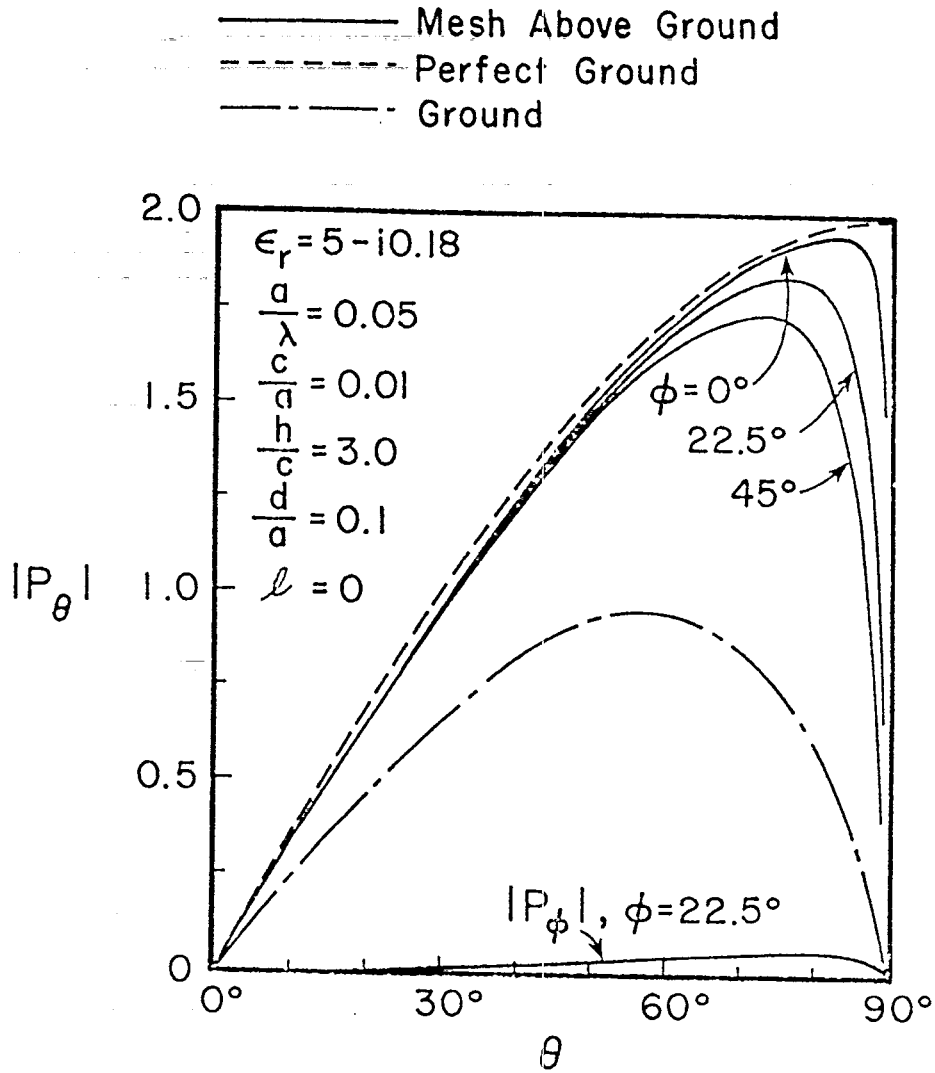
Figure 18　Magnitude of the vertical (z-directed) dipole pattern for $\ell = 0$.
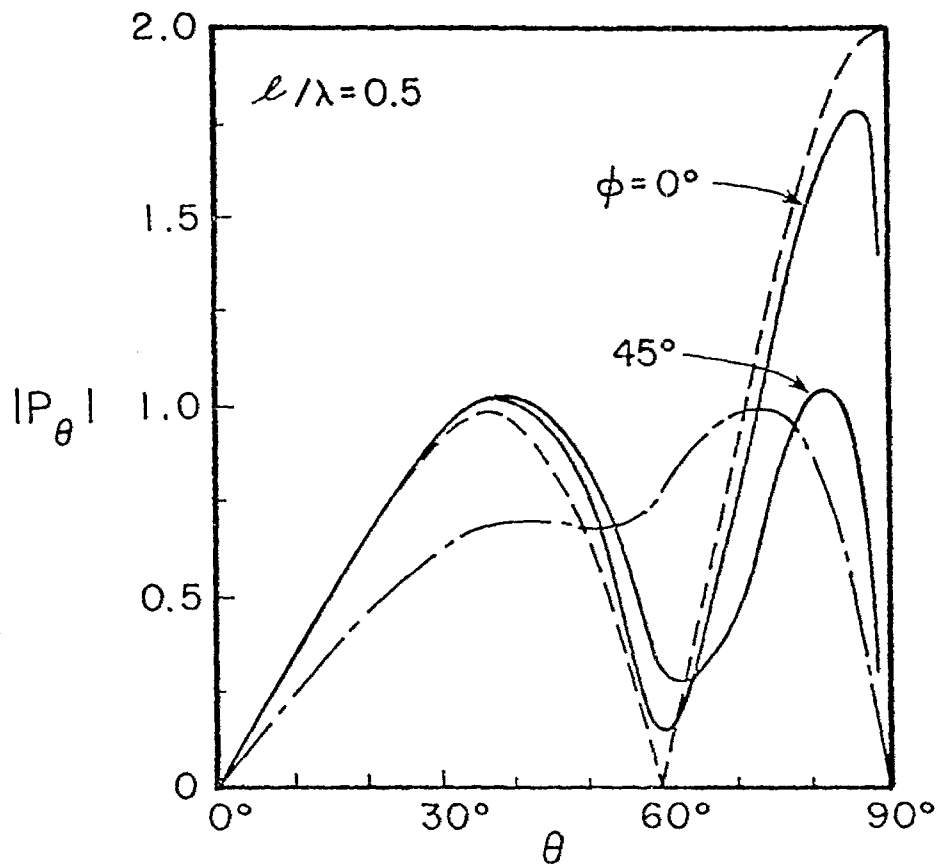
Figure 19   Magnitude of the vertical dipole pattern for $\ell/\lambda = 0.5$.

The radiation patterns of a horizontal dipole (x-directed) are shown for the end-on ($\phi=0°$) and the broadside ($\phi=90°$) directions in Figs. 20 and 21. The dipole is elevated ($\ell/\lambda=0.25$) so that a maximum occurs directly overhead ($\theta=0°$). For $\phi = 0°$, $P_\phi = 0$, and for $\phi = 90°$, $P_\theta = 0$. For comparison, the results for ground alone and perfect ground alone are again shown.

CONCLUDING REMARKS

The numerical results show in a quantitative manner how a wire mesh above the ground surface will reflect electromagnetic waves incident from above. However, it appears that the reflection efficacy is somewhat degraded if the mesh is located very close to the ground surface.

Rectangular mesh calculations have been shown to agree well with the average boundary condition method for sufficiently small spacings. A significant point here is that the rectangular mesh produces greater cross polarization than the square mesh, presumably because it has less symmetry. Unlike the square mesh, there is no azimuthal angle ϕ where the bonded and unbonded rectangular mesh produce the same $R_{\theta\theta}$. Consequently, it may be worthwhile to extend this treatment to the case of the bonded rectangular mesh since such meshes are sometimes used in practice. We may anticipate that even in this case, bonding the mesh degrades the reflecting properties. However, in dealing with very wideband fields, certain practical considerations, such as finite mesh extent at low frequencies or grating lobes at high frequencies, could justify bonding.
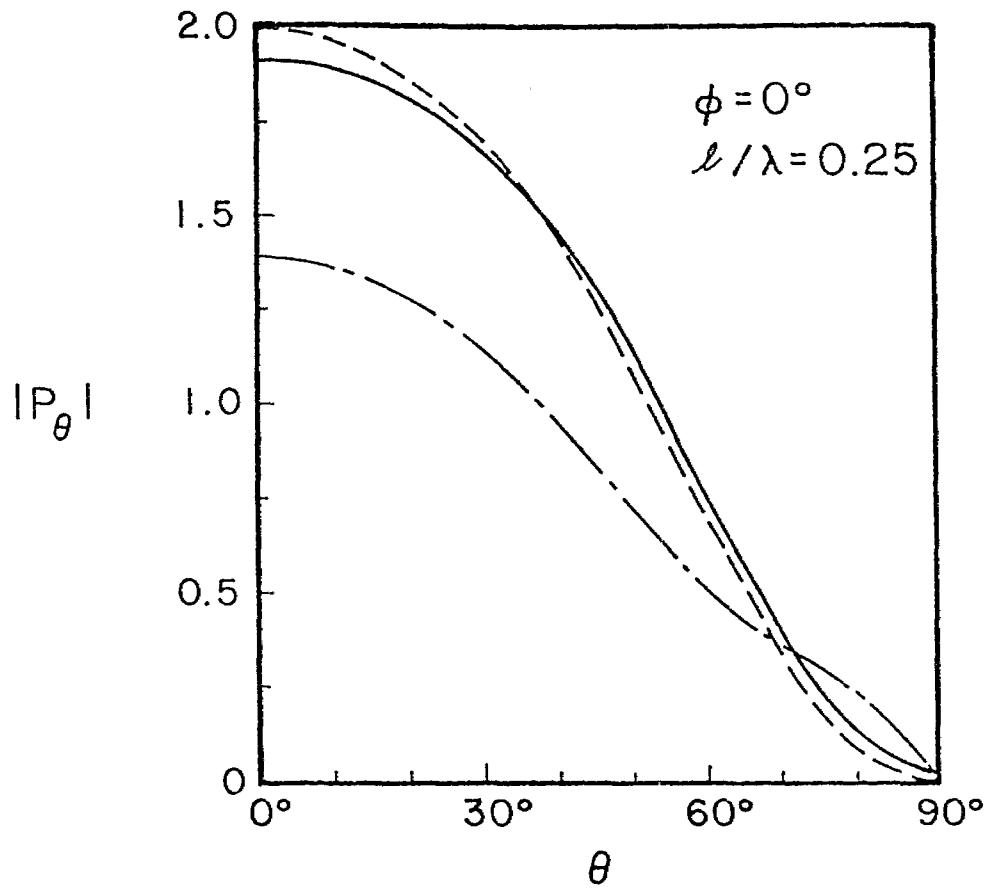
Figure 20   Magnitude of the horizontal (x-directed) dipole pattern off the
end ($\phi = 0^{o}$).
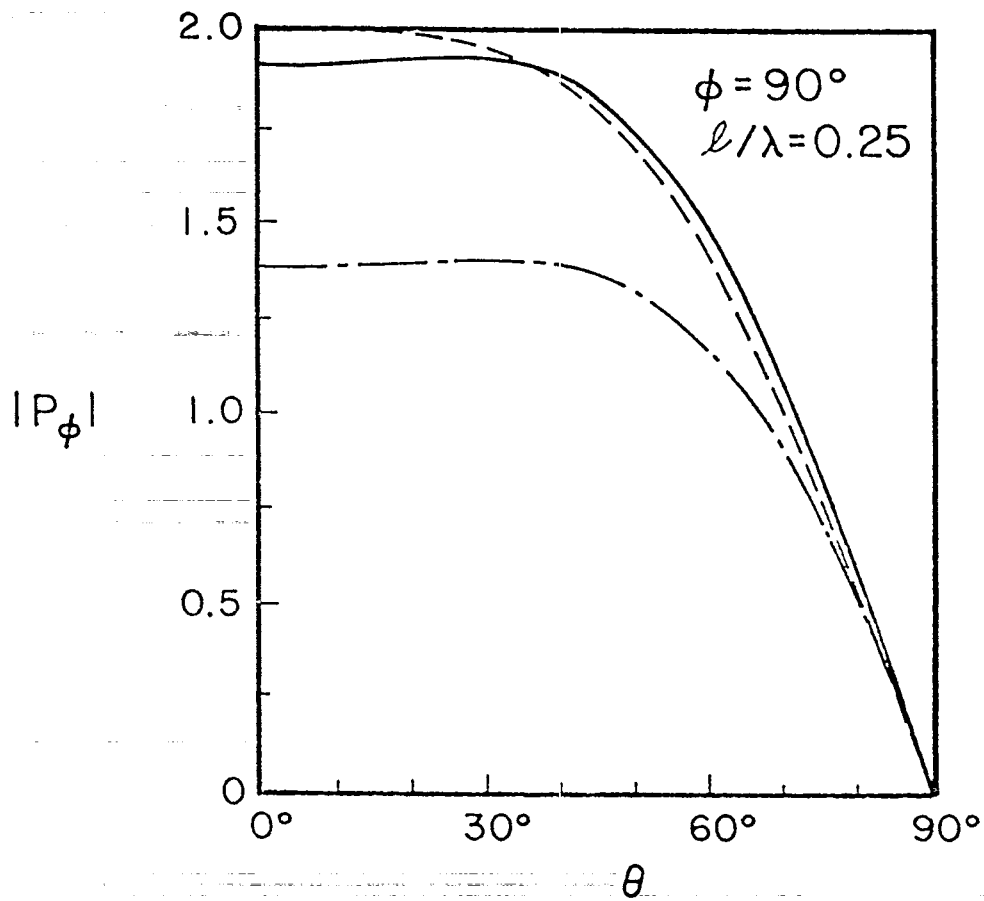
Figure 21   Magnitude of the horizontal dipole pattern at broadside ($\phi = 90°$).

REFERENCES

1　von Ignatowski, W., "Zur theorie der gitter", *Ann. Phys.* (Leipzig), 44, pp. 369, 1914.

2　Gans, R., "Dasverhalten hertzacher gitter", *Ann. Phys.* (Leipzig), 61, pp. 247, 1920.

3　Wessel, W., "Uber den durchgang elektrisher wellen durch draktgitter", *Hochfreq. Electrok.*, 54, pp. 62, 1939.

4　MacFarlane, G.G., "Surface impedance of an infinite parallel-wire grid at oblique angles of incidence", *Proc. IEE*, 93, pp. 1523-1527, 1946.

5　Wait, J.R., "Reflection at arbitrary incidence from a parallel wire grid", *Appl. Sci. Res. B*, 4, pp. 393-400, 1954.

6　Wait, J.R., "Reflection from a wire grid parallel to a conducting plane", *Can. J. Phys.*, 32, pp. 571-579, 1954.

7　Wait, J.R., "The impedance of a wire grid parallel to a dielectric interface", *IRE Trans. Microwave Theory Tech.*, 5, pp. 99-102, 1957.

8　Wait, J.R., "On the theory of reflection from a wire grid parallel to an interface between homogeneous media (II)", *Appl. Sci. Res. B*, 7, pp. 355-360, 1959.

9　Wait, J.R., "Effective impedance of a wire grid parallel to the earth's surface", *IRE Trans. Antennas Propagat.*, 10, pp. 538-542, 1962.

10　Kvavadze, D.K., V.P. Kopaleyshvili, and R.S. Popovidi, "Diffraction of electromagnetic waves on an infinite array placed above a dielectric layer of finite thickness", *Radio Engr. Elect. Phys.*, 7, pp. 1184-1188, 1970.

11　Kontorovich, M.I., V. Yu. Petrun'kin, N.A. Yesepkina, and M.I. Astrakhan, "The coefficient of reflection of a plane electromagnetic wave from a plane wire mesh", *Radio Engr. Elect. Phys.*, 7, pp. 222-231, 1962.

12 Astrakhan, M.I., "Reflecting and screening properties of plane wire grids", *Telecom. Radio Engr.*, 23, pp. 76-83, 1968.

13 Kontorovich, M.I., "Averaged boundary conditions on the surface of a lattice with rectangular cells", *Radio Engr. Elect. Phys.*, 8, pp. 1239-1241, 1963.

14 Otteni, G.A., "Plane wave reflection from a rectangular mesh ground screen", *IEEE Trans. Antennas Propagat.*, AP-21, pp. 843-851, 1973.

15 Hill, D.A. and J.R. Wait, "Electromagnetic scattering of an arbitrary plane wave by two nonintersecting perpendicular wire grids", *Can. J. Phys.*, 52, pp. 227-237, 1974.

16 Collin, R.E., *Field Theory of Guided Waves*, McGraw-Hill Book Co., New York, 1960, p. 368.

17 Mittra, R., *Computer Techniques for Electromagnetics*, Pergamon, Oxford, 1973.

18 Papoulis, A., *The Fourier Integral and its Applications*, McGraw-Hill Book Co., New York, 1962, p. 30.

19 Mittra, R. and W.L. Ko, "A finite difference approach to the wire junction problem", *IEEE Trans. Antennas Propagat.*, AP-23, pp. 435-438, 1975.

20 King, R.W.P. and T.T. Wu, "Analysis of crossed wires in a plane wave field", *Interaction Note 216*, 1974.

21 Butler, C.M., "Currents induced on a pair of skew crossed wires", *IEEE Trans. Antennas Propagat.*, AP-20, pp. 731-736, 1972.

22 Taylor, C.D., L.M. Lin, and H.V. McAdams, "Scattering from crossed wires", *IEEE Trans. Antennas Propagat.*, AP-18, pp. 133-136, 1970.

23 Chao, H.H. and B.J. Strait, "Radiation and scattering by bent wires", *IEEE Trans. Antennas Propagat.*, AP-19, pp. 701-702, 1971.

24 Hill, D.A. and J.R. Wait, "Electromagnetic scattering of an arbitrary plane wave by a wire mesh with bonded junctions", Section II of this report and also *Can. J. Phys.*, 54, pp. 353-361, 1976.

25 Baum, C.E., "Interaction of electromagnetic fields with an object which has an electromagnetic symmetry plane", *Interaction Note 63*, 1971.

26 Hamming, R.W., *Numerical Methods for Scientists and Engineers*, McGraw-Hill Book Co., New York, 1973, pp. 62-63.

27 Kontorovich, M.I., M.I. Astrakhan, and M.N. Spirina, "Slowing down of electromagnetic waves by wire meshes", *Radio Engr. Elect. Phys.*, 9, pp. 1242-1245, 1964.

28 Wait, J.R., "The electromagnetic fields of a dipole in the presence of a thin plasma sheet", *Appl. Sci. Res. B*, 8, pp. 397-417, 1961.

29 Wait, J.R., "Propagation of electromagnetic waves along a thin plasma sheet", *Can. J. Phys.*, 38, pp. 1586-1595, 1960.

30 Wait, J.R. and D.A. Hill, "Electromagnetic scattering by two perpendicular wire grids over a conducting half-space", Section IV of this report and also *Radio Science*, 11, pp. 725-730, 1976.